CaMK1D signalling in AgRP neurons promotes ghrelin-mediated food intake

Karl Vivot, Gergö Meszaros, Evanthia Pangou, Zhirong Zhang, Mengdi Qu, Eric Erbs, Gagik Yeghiazaryan, Mar Quiñones, Erwan Grandgirard, Anna Schneider, et al.

CaMK1D signaling in AgRP neurons promotes ghrelin-mediated food intake

Karl Vivot[1,2,3,4#], Gergö Meszaros[1,2,3,4], Evanthia Pangou[1,2,3,4], Zhirong Zhang[1,2,3,4], Mengdi Qu[1,2,3,4], Eric Erbs[1,2,3,4], Gagik Yeghiazaryan[5], Mar Quiñones[6,7], Erwan Grandgirard[1,2,3,4], Anna Schneider[1,2,3,4], Etienne Clauss--Creusot[4,8], Alexandre Charlet[4,8], Maya Faour[9], Claire Martin[9], Fedor Berditchevski[10], Izabela Sumara[1,2,3,4], Serge Luquet[9], Peter Kloppenburg[5], Ruben Nogueiras[6,11], and Romeo Ricci[1,2,3,4,12#]

[1]Institut de Génétique et de Biologie Moléculaire et Cellulaire, Illkirch 67404, France

[2]Centre National de la Recherche Scientifique, UMR7104, Illkirch 67404, France

[3]Institut National de la Santé et de la Recherche Médicale, U964, Illkirch 67404, France

[4]Université de Strasbourg, Strasbourg 67081, France

[5]Biocenter, Institute for Zoology, and Cologne Excellence Cluster on Cellular Stress Responses in Aging-Associated Diseases (CECAD), University of Cologne, Cologne 50674, Germany

[6]Instituto de Investigación Sanitaria de Santiago de Compostela, Complexo Hospitalario Universitario de Santiago (CHUS/SERGAS), Travesía da Choupana s/n, 15706, Santiago de Compostela, Spain.

[7]CIBER Fisiopatología de la Obesidad y Nutrición (CIBERobn), Instituto de Salud Carlos III, Santiago de Compostela 15706, Spain

[8]Centre National de la Recherche Scientifique, Institute of Cellular and Integrative Neurosciences, Strasbourg 67084, France

[9]Université Paris Cité, CNRS, Unité de Biologie Fonctionnelle et Adaptative, F-75013 Paris, France

[10]Institute of Cancer and Genomic Sciences, The University of Birmingham, Birmingham B15 2TT, United Kingdom

[11] Department of Physiology, CIMUS, University of Santiago de Compostela-Instituto de Investigación Sanitaria, Santiago de Compostela 15782, Spain.

[12]Laboratoire de Biochimie et de Biologie Moléculaire, Nouvel Hôpital Civil, Strasbourg 67091, France

[#]Correspondance: romeo.ricci@igbmc.fr and vivotk@igbmc.fr

Abstract

Hypothalamic AgRP/NPY neurons are key players in the control of feeding behavior. Ghrelin, a major orexigenic hormone activates AgRP/NPY neurons to stimulate food intake and adiposity. However, cell-autonomous ghrelin-dependent signaling mechanisms in AgRP/NPY neurons remain poorly defined. Here we show that calcium/calmodulin-dependent protein kinase ID (CaMK1D), a genetic hot spot in type 2 diabetes, is activated upon ghrelin stimulation and acts in AgRP/NPY neurons to mediate ghrelin-dependent food intake. Global *CaMK1D* knockout male mice are resistant to ghrelin, gain less body weight and are protected against high-fat diet-induced obesity. Deletion of *CaMK1D* in AgRP/NPY but not in POMC neurons is sufficient to recapitulate above phenotypes. In response to ghrelin, lack of CaMK1D attenuates phosphorylation of CREB and CREB-dependent expression of the orexigenic neuropeptides AgRP/NPY in fiber projections to the paraventricular nucleus (PVN). Hence, CaMK1D links ghrelin action to transcriptional control of orexigenic neuropeptide availability in AgRP neurons.

Main

The central nervous system (CNS) orchestrates a complex array of processes mediating energy intake and expenditure. Hormonal, neuronal and nutritional signals according to changes in food absorption, energy storage and energy consumption in different organs reach the CNS which in turn triggers corresponding changes in feeding behavior and peripheral cellular metabolism[1].

Sensing of the nutrient status of the organism is governed by distinct neuronal cell populations, particularly within the arcuate nucleus (ARC) of the hypothalamus[2]. Neurons in this region provide specific projections to other hypothalamic nuclei including the paraventricular nucleus of the hypothalamus (PVN) or to different extrahypothalamic brain regions that in turn coordinate corresponding behavioral responses[3].

Orexigenic neuropeptide Y (NPY) and agouti-related peptide (AgRP)-expressing -neurons and anorexigenic proopiomelancortin (POMC)-expressing neurons in the arcuate nucleus of the hypothalamus are primarily involved in the regulation of energy homeostasis. Leptin, ghrelin and insulin emerged as key hormones in this context. Both leptin and insulin receptors are expressed in these neurons and they have been found to activate POMC neurons and to inhibit AgRP/NPY neurons[4]. Ghrelin enhances the activity of AgRP/NPY neurons via its receptors, while it decreases the activity of POMC neurons through a ghrelin receptors-independent mechanism[5].

Dysfunction of these neuronal circuits contributes to overnutrition and obesity that eventually culminates in type 2 diabetes (T2D)[6]. Obesity and T2D are interlinked and complex metabolic disorders. Recent genome-wide association studies (GWAS) and GWAS meta-analyses revealed complex polygenic factors influencing the development of both diseases. In fact, more than ~250 genetic loci have been identified for monogenic, syndromic, or common forms of

T2D and/or obesity-related traits[7,8]. The contribution of single nucleotide polymorphism (SNPs) to the pathogenesis of these diseases remains largely elusive.

CDC123 (cell division cycle protein 123)/CaMK1D (calcium/calmodulin-dependent protein kinase 1D) represents one such locus on chromosome 10, strongly associated with T2D in European and Asian populations[9–11]. Among other variants, fine mapping identified rs11257655 as the predominant SNP within this locus[12]. The change from C to T in the enhancer region of the rs11257655 allele, promotes DNA hypomethylation and the binding of the transcription factors FOXA1/FOXA2 on the enhancer region resulting in enhanced CaMK1D gene transcription[13,14]. Thus, CaMK1D expression might be enhanced and contributes to the development of T2D. The genetic association of the *CaMK1D* locus with T2D and correlation of clinical data revealed that CaMK1D might promote pancreatic β cell dysfunction[15]. However, direct experimental evidence for the latter conclusion is lacking thus far. Another study proposed that CaMK1D stimulates hepatic glucose output, a mechanism contributing to T2D[16].

CaMK1D (or CaMK1δ) is the fourth member of the CaMK1 subfamily. These kinases have been mainly shown to be important in neurons. CaMK1s control neuron morphology[17] including axonal extension, growth cone motility[18] and dendritogenesis[19]. It has been demonstrated that CaMK1s may also regulate neuronal function by controlling the long-term potentiation, a process involving persistent strengthening of synapses that leads to a long-lasting increase in signal transmission among neurons[20]. However, specific non-redundant neuronal functions of any of the four members of the CaMK1 subfamily including CaMK1D have yet to be determined.

Using global and conditional *CaMK1D* knockout mice, we provide evidence for a role of CaMK1D in central regulation of food intake, while its function seems to be dispensable in the

liver and in the pancreatic β cell in this context. We demonstrate that CaMK1D acts in hypothalamic AgRP neurons to control food intake in response to ghrelin. While CaMK1D in AgRP neurons is dispensable for ghrelin-stimulated increase in electrical neuronal activity and AMPK signaling, its absence reduces ghrelin-induced activatory CREB phosphorylation, AgRP transcription and AgRP/NPY abundance within the PVN. Our data thus unveil a ghrelin signaling mechanism in AgRP neurons to be necessary for efficient appetite stimulation.

Results

CaMK1D$^{-/-}$ mice are protected against obesity

To understand the function of CaMK1D in metabolism, we generated mice carrying a floxed allele of *CaMK1D* (Extended Data Fig. 1a-b) and crossed them with the global Cre-mediated deleter, Rosa26-Cre[21], to obtain whole-body knockout mice. Western blotting confirmed efficient deletion of *CaMK1D* in different organs including brain, pancreas and intestine (Fig. 1a). Whole-body *CaMK1D* knockout mice (*CaMK1D*$^{-/-}$ mice) were born in expected gender distribution (Extended Data Fig. 1c) and Mendelian ratios (Extended Data Fig. 1d) and developed without overt problems. Body and tibia lengths at 7 weeks of age were equal in *CaMK1D*$^{-/-}$ and wild type mice (*CaMK1D*$^{+/+}$ mice) (Extended Data Fig. 1e and 1f), thus excluding any major postnatal growth defect. However, body weight in *CaMK1D*$^{-/-}$ mice on a chow diet was significantly reduced at 21 weeks of age as compared to *CaMK1D*$^{+/+}$ mice. This difference was exacerbated when obesity was induced in mice on a high fat diet (HFD) reaching statistical significance at the age of 18 weeks (Fig.1b). Quantitative Nuclear Magnetic Resonance (qNMR) revealed that HFD-fed *CaMK1D*$^{-/-}$ mice, compared to *CaMK1D*$^{+/+}$ mice, had reduced fat mass, while there was no significant difference in the lean mass and free body fluid (FBF) (Fig. 1c). *Leptin*-deficient mice (*ob/ob* mice) lacking CaMK1D also showed reduced body weight as compared to *ob/ob* mice, reaching statistic significance at the age of 14 weeks (Fig. 1d).

In line with reduced diet-induced obesity, fasting glucose levels in 14 weeks old *CaMK1D*$^{-/-}$ mice on a HFD was significantly reduced as compared to control *CaMK1D*$^{+/+}$ mice (Figure 1e). In fact, glucose levels in *CaMK1D*$^{-/-}$ mice on a HFD were similar as in corresponding chow diet-fed mice indicating that they were protected from obesity-induced hyperglycemia. There was no apparent difference in fasting glucose levels between *CaMK1D*$^{-/-}$ and *CaMK1D*$^{+/+}$ mice on a chow diet (Figure 1e). The observed reduced fasting glucose levels correlated with reduced

fasting insulin levels (Figure 1f). Glucose tolerance was slightly, but not significantly, improved in *CaMK1D*$^{-/-}$ as compared to CaMK1D$^{+/+}$ mice on a chow diet (Fig. 1g). However, these differences became significant in mice on a HFD (Fig 1h and 1i). While insulin tolerance was unaltered in *CaMK1D*$^{-/-}$ mice on a chow diet (Figure 1j), it was significantly improved in *CaMK1D*$^{-/-}$ mice as compared to *CaMK1D*$^{+/+}$ mice on a HFD (Figure 1k and 1l). Glucose-induced secretion of insulin (GSIS) was slightly but not significantly reduced in *CaMK1D*$^{-/-}$ mice as compared to *CaMK1D*$^{+/+}$ mice on a HFD (Extended Data Fig. 2a). GSIS from isolated islets of *CaMK1D*$^{-/-}$ and *CaMK1D*$^{+/+}$ mice was comparable (Extended Data Fig. 2b).

To further exclude a primary role of CaMK1D in the pancreas including β cells, we crossed floxed mice with *PDX1*$^{Cre/+}$ mice[22]. Western blotting confirmed that deletion of *CaMK1D* in the pancreas was efficient, while no apparent deletion was visible in brain (Extended Data Fig. 2c). Pancreas-specific *CaMK1D* knockout mice (*PDX1*$^{Cre/+}$*;CaMK1D*$^{flox/flox}$ mice) did not show any differences in body weight and glucose tolerance as compared to floxed control mice (*CaMK1D*$^{flox/flox}$ mice) on a chow diet as well as HFD (Extended Data Fig. 2d-f), confirming that CaMK1D is dispensable in β cell function.

Hepatic insulin resistance leading to increased gluconeogenesis is an important mechanism contributing to obesity-related changes in glucose homeostasis[23]. Therefore, we generated liver-specific *CaMK1D* knockout mice (*Alb*$^{Cre/+}$*;CaMK1D*$^{flox/flox}$ mice) using *Albumin*$^{Cre/+}$ mice[24] and corresponding floxed control mice (*CaMK1D*$^{flox/flox}$ mice). Quantitative reverse transcription PCR (qRT-PCR) confirmed efficient deletion of *CaMK1D* in the liver (Extended Data Fig. 2g). However, hepatic deletion of *CaMK1D* did not affect body weight ~~gain~~, glucose tolerance and insulin tolerance in mice on a chow diet as well as on HFD (Extended Data Fig. 2h-l). Thus, our data exclude any major functions of CaMK1D in pancreatic β cells and liver under both normal and obesity conditions.

Deletion of *CaMK1D* alters ghrelin-mediated food intake

To further understand reduced body weight and fat mass in *CaMK1D*$^{-/-}$ mice as compared to *CaMK1D*$^{+/+}$ mice, we next explored energy metabolism. In line with reduced body weight, cumulative food intake was decreased in *CaMK1D*$^{-/-}$ mice as compared to *CaMK1D*$^{+/+}$ mice on a chow diet as well as on HFD, reaching statistical significance at 20 weeks of age (Fig. 2a and b). Cumulative food intake was also reduced in *ob/ob* mice lacking *CaMK1D* as compared to *ob/ob* mice, reaching statistical significance at the age of 12 weeks (Fig. 2c). Likewise, cumulative food intake after 24 hours fasting was significantly reduced in *CaMK1D*$^{-/-}$ mice throughout the observed period of refeeding as compared to *CaMK1D*$^{+/+}$ mice (Fig. 2d).

Indirect calorimetry revealed that energy expenditure was equal in *CaMK1D*$^{-/-}$ mice as compared to *CaMK1D*$^{+/+}$ mice on a HFD. Indeed, the regression-based analysis-of-covariance (ANCOVA) showed that there was no body weight-independent metabolic rate (MR) difference in the *CaMK1D*$^{-/-}$ mice relative to *CaMK1D*$^{+/+}$ mice (Fig. 2e). However, locomotor activity of *CaMK1D*$^{-/-}$ as compared to *CaMK1D*$^{+/+}$ mice was significantly reduced at the beginning of the night period after 24 hours fasting (Fig. 2f and 2g) in line with reduced appetite and reduced seeking for food in response to fasting. Thus, reduced obesity primarily correlated with reduced appetite and food intake.

Ghrelin is a gut-derived hormone released in response to fasting and promotes feeding behavior and adiposity[25]. Given that the resistance to diet-induced obesity of *CaMK1D*$^{-/-}$ mice could be explained by reduced food intake, we next wondered whether the ghrelin response was affected in mice lacking *CaMK1D*. To this end, we determined cumulative food intake upon intraperitoneal injections of ghrelin in mice on a chow diet. While *CaMK1D*$^{+/+}$ mice showed a significant increase in cumulative food intake at 4 and 6 hours after ghrelin injection, such response was almost absent in *CaMK1D*$^{-/-}$ mice (Fig. 2h). In contrast, the response to leptin was comparable in *CaMK1D*$^{+/+}$ mice and *CaMK1D*$^{-/-}$ mice (Fig. 2i). Blood levels of acylated

ghrelin were significantly higher in *CaMK1D*$^{-/-}$ as compared to *CaMK1D*$^{+/+}$ mice on a HFD (Fig. 2j), suggesting an adaptive response to a primary defect in ghrelin action. Conversely, blood levels of leptin were significantly lower in *CaMK1D*$^{-/-}$ mice as compared to *CaMK1D*$^{+/+}$ mice (Fig. 2k) on a HFD, correlating well with the degree of obesity.

To exclude any major anxiety-like behavior or stress-induced anhedonia, we subjected mice to an open field and to a sucrose preference test, respectively. No major differences between genotypes could be observed (Extended Data Fig. 3a-h). Thus, global deletion of *CaMK1D* results in compromised ghrelin action, which contributes to reduced food intake and body weight.

CaMK1D regulates ghrelin-induced food intake in AgRP neurons

Ghrelin stimulates central neurons to promote feeding. We thus next asked whether CaMK1D in the nervous system was mainly responsible for the observed phenotype in *CaMK1D*$^{-/-}$ mice. We therefore crossed *CaMK1D*$^{flox/flox}$ mice with *Nestin*$^{Cre/+}$ mice resulting in efficient deletion of *CaMK1D* in brain including hypothalamus but not in other organs such as intestine and pancreas (Extended Data Fig. 4a). Indeed, the body weight was significantly attenuated in nervous system-specific *CaMK1D* knockout mice (*Nestin*$^{Cre/+}$;*CaMK1D*$^{flox/flox}$ mice) at the age of 17 weeks as compared to Cre and floxed control mice (*Nestin*$^{Cre/+}$ mice and *CaMK1D*$^{flox/flox}$ mice) on a chow diet as well as on HFD (Extended Data Fig. 4b). Cumulative food intake was decreased in *Nestin*$^{Cre/+}$;*CaMK1D*$^{flox/flox}$ mice at the age of 16 weeks as compared to control mice on a chow diet (Extended Data Fig. 4c) as well as on a HFD (Extended Data Fig. 4d). Likewise, cumulative food intake in after 24 hours fasting was significantly reduced in *Nestin*$^{Cre/+}$;*CaMK1D*$^{flox/flox}$ mice as compared to control mice after 4, 14 and 24 hours of refeeding (Extended Data Fig. 4e). Consistently, while control mice showed a significant

increase in cumulative food intake at 4 and 6 hours after ghrelin injections, such response was absent in *Nestin*$^{Cre/+}$;*CaMK1D*$^{flox/flox}$ mice (Extended Data Fig. 4f).

Ghrelin primarily acts on hypothalamic neurons in the arcuate nucleus. In particular, it stimulates NPY/AgRP neurons to promote appetite [26]. Given our results obtained in nervous system-specific knockout mice, we next asked whether CaMK1D acts in AgRP neurons to control food intake. To this end, we crossed *CaMK1D*$^{flox/flox}$ mice with *AgRP*$^{Cre/+}$ mice resulting in efficient recombination of the *CaMK1D* locus in hypothalamus but not in the brain cortex, liver, tail and white blood cells (Extended Data Fig. 5a). Quantitative RT-PCR experiments revealed 60% reduction in CaMK1D expression in the hypothalamic ARC of AgRP neuron-specific *CaMK1D* knockout mice as compared to control mice. Expression of CaMK1D was unaffected in cortex or liver (Extended Data Fig. 5b). These results confirm significant but not exclusive expression and efficient deletion of CaMK1D in AgRP neurons. Strikingly, AgRP neuron-specific *CaMK1D* knockout mice (*AgRP*$^{Cre/+}$; *CaMK1D*$^{flox/flox}$ mice) at the age of 18 weeks showed significantly less body weight as compared to Cre and floxed control mice (*AgRP*$^{Cre/+}$ mice and *CaMK1D*$^{flox/flox}$ mice) on a chow diet as well as on HFD (Fig. 3a). Similar to nervous system-specific knockout mice, *AgRP*$^{Cre/+}$; *CaMK1D*$^{flox/flox}$ mice showed significantly less cumulative food intake as compared to control mice on a chow diet (Fig. 3b) as well as HFD (Fig. 3c). Similar significant differences were observed in the cumulative food intake after 24 hours fasting (Fig. 3d) as well as in response to ghrelin injection (Fig. 3e). To confirm a role of CaMK1D in AgRP neurons of adult mice, we delivered AAVs carrying a Cre-driven expression cassette of shRNA against CaMK1D (AAV-DIO-shCaMK1D-EGFP) or scramble shRNA (AAV-DIO-scramble-EGFP) into the ARC of AgRP-Cre mice by stereotaxic injection. EGFP-expressing cells were also AgRP-positive confirming proper targeting (Fig. 3f). We found impaired ghrelin-induced food intake in *shCaMK1D*-expressing AAVs-injected as compared to control AAVs-injected mice (Fig. 3g). We also used stereotaxic

delivery of AAVs carrying a Cre-driven expression cassette of CaMK1D (AAV-DIO-CaMK1D-eGFP) or AAV-DIO-eGFP in *AgRP*$^{Cre/+}$; *CaMK1D*$^{flox/flox}$ mice and *AgRP*$^{Cre/+}$ control mice. EGFP-expressing cells were also AgRP-positive confirming proper targeting using stereotaxis (Fig. 3h). Quantitative RT-PCR in ARC, VMH and Cortex verified very efficient and specific CaMK1D re-expression (Fig. 3i). Ghrelin-induced food intake was significantly attenuated in *AgRP*$^{Cre/+}$; *CaMK1D*$^{flox/flox}$ mice as compared to *AgRP*$^{Cre/+}$ control mice before AAV injections (Fig. 3j). Re-expression of *CaMK1D*-EGFP in AgRP neurons lacking *CaMK1D* restored ghrelin-induced food intake in the same mice (Fig. 3k), while expression of CaMK1D in AgRP neurons of control mice had no additive effect. eGFP expression alone did not affect food intake in response to ghrelin (Fig. 3k). This suggests that CaMK1D acts specifically in adult AgRP neurons to control ghrelin-induced food intake, excluding an irreversible developmental defect. To further exclude major developmental defects, we next employed the DREADD approach (hM3Dq receptor expression) in *AgRP*$^{Cre/+}$;*CaMK1D*$^{flox/flox}$ mice. DREADD activation is known to lead to a supraphysiologic activation of AgRP neurons bypassing subtle receptor mediated activation. Indeed, we found that food intake induced by the agonist Clozapine N-oxide (CNO) was not affected in mice lacking CaMK1D in AgRP neurons (Fig. 3l-m). Importantly, responses to ghrelin did not change upon deletion of *CaMK1D* in anorexigenic POMC neurons (Extended Data Fig. 6a–f), suggesting that the effects of CaMK1D on food intake are specific to AgRP neurons.

To further evaluate a role of CaMK1D in AgRP neuron-dependent energy metabolism, we next performed indirect calorimetry with *AgRP*$^{Cre/+}$;*CaMK1D*$^{flox/flox}$ mice and control mice on a chow diet. Although the cumulative food intake (Fig. 4a) was reduced in *AgRP*$^{Cre/+}$;*CaMK1D*$^{flox/flox}$ mice as compared to control mice, the locomotor activity (Fig. 4b and 4c) was unchanged. The regression-based analysis-of-covariance (ANCOVA) confirmed that there was a body weight-independent metabolic rate (MR) difference with lower MR in

the *AgRP*$^{Cre/+}$;*CaMK1D*$^{flox/flox}$ relative to the control mice on a chow diet (Fig. 4d). Given the overall reduction in body weight, reduced energy expenditure was most likely compensatory to compromised energy availability caused by reduced food intake. Altogether, our data thus suggest that CaMK1D acts in AgRP neurons to primarily control food intake in response to ghrelin.

Deletion of CaMK1D does not affect AgRP/NPY neuron activity

C-fos expression is used as a marker for neuronal activity [27]. To understand the function of CaMK1D in ghrelin-induced neuronal activity, we next explored c-fos expression in NPY/AgRP neurons in the absence and presence of CaMK1D using NPY-GFP reporter mice[28]. No differences in basal and ghrelin-induced c-fos expression in NPY-GFP expressing cells in the ARC of *CaMK1D*$^{-/-}$ and *CaMK1D*$^{+/+}$ mice on a chow diet were found (Fig. 5a and 5b). To verify this finding, we compared the effect of ghrelin on AgRP neurons between both mouse lines using perforated patch clamp recordings in brain slices. To identify AgRP neurons, we generated *CaMK1D*$^{-/-}$ and *CaMK1D*$^{+/+}$ mice carrying a EGFP reporter under the control of the *AgRP* promoter (*CaMK1D*$^{-/-}$-AgRP-EGFP and *CaMK1D*$^{+/+}$-AgRP-EGFP mice) (Fig. 5c). The ghrelin-induced increases in action potential frequency were similar in AgRP neurons of *CaMK1D*$^{-/-}$-AgRP-EGFP as compared to *CaMK1D*$^{+/+}$-AgRP-EGFP mice (*CaMK1D*$^{+/+}$, n=12; *CaMK1D*$^{-/-}$, n=10, p=0.82) (Fig. 5d and 5e). Between the two mouse lines, we also found no significant differences in general intrinsic electrophysiological properties of AgRP neurons such as spontaneous actions potential frequency, input resistance, excitability, and whole-cell capacitance (Fig. 5f-i). Taken together, these data suggest that CaMK1D is dispensable for ghrelin-stimulated activation of AgRP neurons.

Ghrelin activates CaMK1D to induce AgRP/NPY expression

Lack of CaMK1D did not affect ghrelin-induced increase in electrical activity of AgRP neurons prompting us to hypothesize that CaMK1D acts downstream or independent of neuronal activity. We thus next asked whether CaMK1D is activated upon ghrelin. We first used Phos-tag gels to address CaMK1D phosphorylation in response to ghrelin in cultured primary hypothalamic cells isolated from *CaMK1D*$^{-/-}$ and *CaMK1D*$^{+/+}$ mice. Indeed, phosphorylated CaMK1D as marked by the upshifted band increased upon ghrelin stimulation (Fig. 6a). Calcium/calmodulin directly activates calcium/calmodulin-dependent protein kinase I by binding to the enzyme and indirectly promotes the phosphorylation and synergistic activation of the enzyme by calcium/calmodulin-dependent protein kinase kinase (CaMKK) [29]. In line with above findings in cultured neurons, activatory phosphorylation of CaMK1D significantly increased in hypothalamus of ghrelin-stimulated *CaMK1D*$^{+/+}$ mice, while no phosphorylation of CaMK1D or total protein was visible in *CaMK1D*$^{-/-}$ samples (Fig. 6b and c). Thus, ghrelin activates CaMK1D in hypothalamic cells.

Ghrelin stimulates AMPK activity in the hypothalamus[30]. However, ghrelin-induced AMPK activity was equal in primary hypothalamic neurons of *CaMK1D*$^{-/-}$ and *CaMK1D*$^{+/+}$ mice as shown by assessment of activatory phosphorylation of AMPK and phosphorylation of its target acetyl-CoA carboxylase (ACC) (Fig. 6d-f). Ghrelin-induced cAMP response element (CRE)-binding protein (CREB) phosphorylation promotes expression of AgRP and NPY that mediate the orexigenic action of ghrelin[31]. To monitor phosphorylation of CREB in response to ghrelin, we used immunofluorescence in the ARC of NPY-GFP reporter mice. NPY-GFP positive neurons of *CaMK1D*$^{+/+}$ mice showed enhanced phosphorylated CREB in response to ghrelin, while ghrelin-induced phosphorylation was abolished in *CaMK1D*$^{-/-}$ mice (Fig. 6g and h). In line with reduced phosphorylation of CREB, Ghrelin-induced transcription of AgRP and NPY but not POMC was almost abolished in *CaMK1D*$^{-/-}$ cells (Fig. 6i), indicating that reduction of

activatory CREB phosphorylation constitutes at least one plausible explanation for reduced expression of AgRP and NPY. NPY and AgRP projections in the PVN are dynamically regulated in response to ghrelin. While they increased in control mice in response to ghrelin, this increase was completely abolished in *CaMK1D* knockout mice. Importantly, no differences in NPY and AgRP projections was found at baseline suggesting again that a ghrelin-specific response is affected in the absence of CaMK1D (Fig. 6j-m). Reduced levels and thus decreased inhibitory action of AgRP and NPY on predominantly anorexigenic neurons in the PVN is thus a likely mechanism underlying reduced food intake and body weight despite normal AgRP neuronal activity. Hence, CaMK1D in AgRP neurons is required for CREB-dependent expression of the orexigenic neuropeptides AgRP and NPY, thereby regulating food intake and obesity.

Discussion

A possible role of CaMK1D in obesity and T2D has been predicted based on recent GWAS studies. However, the function of CaMK1D in physiology and metabolic disease *in vivo* was unknown thus far. In our study, using a loss-of-function approach in mice, we discovered an unpredicted role of CaMK1D in central control of food intake. We excluded a cell-autonomous role of CaMK1D in the liver and pancreas.

We found that CaMK1D is specifically required in AgRP neurons to promote ghrelin-induced food intake. As genetic studies predicted enhanced expression of CaMK1D to contribute to T2D [13,14], our data also fit with a model in which enhanced CaMK1D signaling in AgRP neurons promotes obesity. Deletion of *CaMK1D* in AgRP neurons is sufficient to trigger significant effects on body weight and food intake seen in global *CaMK1D* knockout mice highlighting the importance of CaMK1D signaling in this subpopulation of neurons.

CaMK1D is widely expressed in the CNS and ghrelin has been reported to act in different hypothalamic and extrahypothalamic areas to induce feeding. Having that said, we showed that CaMK1D is dispensable in anorexigenic POMC neurons. Even though deletion of *CaMK1D* in AgRP neurons largely recapitulates phenotypes seen in whole-body knockout mice, this does not fully exclude functions in other organs implicated in energy homeostasis that needs to be further explored.

Importantly, CaMK1D is dispensable for ghrelin-stimulated electrical activity of AgRP neurons. This finding is in line with a model in which ghrelin-driven neuronal activity induces membrane depolarization and calcium changes which in turn trigger CaMK1D activation and CaMK1D-dependent responses including CREB-dependent transcription[32]. Thus, our study has identified a so far unknown signaling pathway in AgRP neurons that links neuronal activity to CREB-dependent transcription (Fig. 6n).

CREB-dependent transcription has been shown to regulate fundamental processes in neuronal development, activity-dependent dendritic outgrowth, and synaptic plasticity[33]. In AgRP neurons, CREB controls transcription of AgRP and NPY[31]. In accordance with this finding, we found that ghrelin failed to induce AgRP and NPY transcription in *CaMK1D*-deficient hypothalamus and that AgRP and NPY abundance in projections to the PVN were reduced. In fact, it has been demonstrated that ghrelin failed to stimulate feeding upon chemical and genetic inhibition of AgRP and NPY[26,34–37]. Even though AgRP and NPY are crucial neuropeptides inhibiting anorexigenic neurons in the PVN, other CREB-dependent functions might be affected in *CaMK1D*-deficient AgRP neurons that may also contribute to the observed metabolic phenotypes to be investigated in the future. Moreover, CaMK1D might also regulate CREB-independent functions still to be explored.

Deletion of the ghrelin receptor specifically in AgRP neurons[38,39] does not precisely phenocopy body weight phenotypes seen in AgRP neuron specific CaMK1D knockout mice. While they reported apparent differences exclusively in mice on a high fat diet, our study revealed changes in body weight of mice on a chow as well as high fat diet. Therefore, CaMK1D in AgRP neurons might be engaged by other stimuli than ghrelin that are yet to be identified.

Central ghrelin administration induced AMPK phosphorylation and activation and ghrelin responses could be alleviated through AMPK inhibition[40]. AMPK activation was dependent on calcium changes and on CaMKK 2 activation[40]. CaMKK is also known to activate CaMK1 including CaMK1D (Fig. 6G). Interestingly, AMPK activation was shown to occur in the ventro-medial nucleus of the hypothalamus (VMH), since adenoviral delivery of a dominant negative isoform of AMPK into the VMH was sufficient to block ghrelin-induced food intake [40–42]. Therefore, it has been suggested that AgRP/NPY levels in neurons in the ARC are regulated at a presynaptic level by AMPK signaling in neurons of the VMH. We found here that lack of *CaMK1D* almost entirely abolished the increase in AgRP/NPY transcription in

response to ghrelin. Yet, absence of *CaMK1D* does not affect AMPK signaling in response to ghrelin in the hypothalamus. Given that AgRP neuron-specific deletion of *CaMK1D* is sufficient to reduce food intake in response to ghrelin, we propose that the transcriptional control of AgRP/NPY expression primarily depends on CaMK1D signaling in AgRP neurons.

Elevated levels of cAMP led to CREB phosphorylation at serine 133 and mutation of this site abrogated CREB-dependent reporter gene activation [43]. Protein kinase A (PKA) is a main mediator of cAMP-dependent phosphorylation of CREB. Indeed, ghrelin was shown to increase calcium through the cAMP-PKA pathway in NPY-expressing cells in the ARC of rats [44]. However, we observe that phosphorylation of CREB depends, at least partially, on CaMK1D activity. In fact, CREB was shown to be phosphorylated *in vitro* by both kinases, PKA and CaMK1[32]. Given that phosphorylation is reduced but not abolished in the absence of CaMK1D both kinases might be necessary to exert robust CREB phosphorylation in response to ghrelin.

mTOR-S6K1 signaling has also been demonstrated to be involved in hypothalamic regulation of food intake in response to ghrelin through regulation of CREB phosphorylation and AgRP/NPY expression[45,46]. However, it is unclear so far how and in which neurons mTOR-S6K1 regulates ghrelin responses. In fact, mTORC1 signaling in AgRP neurons was shown to control circadian expression of AgRP and NPY but was redundant for regulation of food intake[47].

Altogether, we uncovered a signaling mechanism that acts in AgRP neurons to control levels of AgRP and NPY, two main orexigenic neuropeptides centrally involved in promoting food intake. Uncontrolled CaMK1D signaling in AgRP neurons represents thus a valuable mechanism promoting obesity and T2D.

Methods

Animals Care

Animal care and all experimental procedures done in this study were approved by the local ethical committee (Com'Eth) in compliance with the French and European legislation on care and use of laboratory animals (APAFIS#18638-2019012510177514v4 / APAFIS#21069-2019061411418629v2 / APAFIS#37421-2022052012206789v4). Mice were individually housed under controlled temperature at 22°C and humidity at 40% on a 12H light/dark cycle with unrestricted access to water and prescribed diet. Food was only withdrawn if required for an experiment. Body weight and food intake were determined weekly. Animals were fed with regular chow diet (CD) or high fat diet (HFD). CD contains 73.6% calories from carbohydrates, 18.1% calories from protein, and 8.4% calories from fat (SAFE® D04 from Safe) and HFD contains 20% calories from carbohydrates, 20% calories from protein, and 60% calories from fat (D12492i from Research diet®). For all experiments only male mice were used. All experiments were performed in adult mice at the age between 5-25 weeks.

Generation of Transgenic Mice

CaMK1D conditional knockout and global knockout mice were generated according to the "knockout first" strategy by the Institut Clinique de la Souris (ICS, Illkirch-Graffenstaden, France). 5' of exon 4 of the *CaMK1D* gene a SA-ßGeo-pA (LacZ-neoR) trapping cassette was inserted flanked by two FRT sites, which disrupts gene function (knockout first allele). Furthermore, two LoxP sites were inserted 5' and 3' of exon 4. The FRT-recombinase (Flp) converted the "knockout first" allele to a floxed allele ($CaMK1D^{flox/flox}$), restoring gene activity (Extended Data Fig 1a-b). Verification of correct targeting was done by Southern Blotting as previously described[48]. The sequences of the primers used to genotype the mice and to verify Cre-mediated recombination are provided in Extended Data Table 1. $CaMK1D^{flox/flox}$ mice were mated with Rosa26-Cre mice expressing Cre recombinase under control of the Rosa26

promoter (for global knockout)[21] resulting in the deletion of the floxed exon. The breeding colonies were maintained by mating hemizygote *CaMK1D*$^{+/-}$ females to hemizygote *CaMK1D*$^{+/-}$ males. Mice were on a C57BL/6 N/J mixed background. Tissue-specific deletion of *CaMK1D* was obtained by mating floxed mice with transgenic mice expressing Cre recombinase under the control of a tissue-specific promoter and breeding colonies were maintained by mating tissue-specific promoterCre/+;*CaMK1D*$^{flox/+}$ to *CaMK1D*$^{flox/+}$ mice. All Mice were on a C57BL/6 N/J mixed background. All cre deleter mouse lines are listed in the reporting summary section.

Blood collection and biochemical measurements

Blood samples obtained from the tail and collected in heparinized capillaries were used to measure fasted blood glucose and insulin levels. Animals were fasted at 8 am, and the samples were collected 4 hours later. At the end of the experiment, blood was collected from the retro orbital sinus, put into tubes containing 0.2 μM EDTA and 4 mM Pefabloc® SC, and centrifuged for 15 minutes at 3,000 g to separate the plasma. Plasma was stored at –80°C. Acylated Ghrelin Leptin and Insulin were measured by ELISA.

Glucose and Insulin Tolerance Assays

GTT: After a 16H fast, animals were injected i.p. with 2 g/kg (animals on CD) or 1 g/kg (animals on HFD) dextrose in 0.9% NaCl. Blood glucose was measured prior to and 15, 30, 45, 60, 90, and 120 minutes after injections. Blood glucose values were determined in a drop of blood sampled from the tail using an automatic glucose monitor (Accu-Check; Roche Applied Science). Plasma samples were collected at 0, 15, 30 minutes for insulin measurements.

ITT: After a 5-hour fast, animals were injected i.p. with 0.75 IU/kg recombinant human insulin (Umuline; Lilly®). Blood glucose levels were measured before and 15, 30, 40, 60 and 90 minutes after injections. The glucose disappearance rate for the ITT (kITT) (percentage/minute) was calculated using the formula as previously described[49]. kITT = 0.693 × 100 / t1/2, where t1/2 was calculated from the slope of the plasma glucose concentration, considering an exponential decrement of glucose concentration during the 30 minutes after insulin administration.

Automated Cages Phenotyping for indirect calorimetric measurements

Twenty-five weeks old mice were acclimated in metabolic chambers (TSE LabMaster System - Metabolic Phenotyping Facility, ICS) for 1 day before the start of the recordings. Mice were continuously recorded for 1 or 2 days with measurements of locomotor activity (in the xy- and z-axes), and gas exchange (O_2 and CO_2) every 30 min. Energy expenditure was calculated according to the manufacturer's guidelines (PhenoMaster Software, TSE System). The respiratory quotient was estimated by calculating the ratio of CO2 production to O2 consumption. Values were corrected by metabolic mass (lean mass + 0.2 fat mass) as previously described[50]. ANCOVA analysis was done as previously described[51].

Animal length and body composition

Animal length was assessed with X-Ray MX-20 Specimen (Faxitron - Metabolic Phenotyping Facility, ICS). Digital X-ray pictures allowed the measurement of whole body and tibia size of mice. Body composition was evaluated by Quantitative Nuclear Magnetic Resonance (qNMR) using Minispec$^+$ analyzer (Bruker BioSpin S.A.S., Metabolic Phenotyping Facility, ICS).

Leptin, ghrelin, CNO responsiveness

To assess leptin sensitivity, mice received an i.p. injection of either PBS or mouse recombinant leptin (3 mg/kg) 24H after food withdrawal, their food intake were monitored 4 and 6H following the injections. The food intake after PBS injection was compared with the food intake after leptin administration. The orexigenic response to ghrelin and CNO was determined in mice that received an i.p injection of either PBS or ghrelin (1 mg/kg) / CNO (0.6mg/kg). Food intake was assessed 4H and 6H after injections.

Culture of primary cells of hypothalamus

Hypothalamus were dissected from E15.5 embryos and stored on ice in Neurobasal medium (GIBCO). Tissues were incubated for 20 min in a 37°C water bath in 100U/ml papaïn (Worthinghton) and 10mg/ml DNAse I (Worthinghton). Digestion was stopped with Ovomucoïde (Worthinghton). Tissues were transferred into 1 ml of adult neuronal growth medium consisting of Neurobasal-A medium, 3mM L-glutamine (Gibco) , 1x B-27 supplement, 1x N2 supplement and antibiotics. Tissues were gently triturated until uniform cellular dissociation was achieved. Cells were counted and plated into cell culture plates coated with poly-L-lysine (Gibco).

Western blotting

Cells were washed with ice-cold PBS on ice and snap-frozen in liquid nitrogen. Cell lysates for WB were prepared using 1x Laemmli buffer (50 mM Tris-HCl pH6.8, 100 mM DTT, 8% SDS, 0,01% bromophenol blue, 10% glycerol) supplemented with phosphatase/protease inhibitors (Cell Signaling Technology) and incubated on ice for 10 minutes. After centrifugation at 16 000 g for 10 minutes at 4°C cleared supernatant was transferred to the new tubes and was used immediately stored at −80°C until used. Total protein was measured using the BCA method by Pierce™ BCA Protein Assay Kit (ThermoFisher). Samples (20-50 µg of total protein content)

were boiled and resolved on 10% acrylamide gels using standard Tris-Glycine SDS-PAGE or Phostag gels. Proteins were transferred to PVDF membranes (Millipore) and blotted with antibodies listed in the Antibodies section. For membrane blocking and primary antibody dilution 5% BSA (w/v) in TBST was used. All incubations with primary antibodies were performed for 16 hours at 4°C. Blots were developed using SuperSignal West Pico (Pierce, Ref. 34580) or Luminata Forte Western HRP substrate (Merck Millipore, Ref. WBLUF0500).

Hypothalamic mRNA quantification

Total RNA from hypothalamus was extracted using an RNeasy Lipid Tissue Mini Kit (QIAGEN) and quantified spectrophotometrically. Single-stranded cDNA was synthesized using SuperScript IV RNase Reverse Transcriptase (Invitrogen) according to the manufacturer's directions. Real-time PCR was carried out using an LightCycler® 480 (Roche) with Fast SYBR® Green Master Mix (Roche) and the primers listed in the primers section. Quantifications were done according the Pfaffl method[52].

Immunohistochemistry

Mediobasal hypothalamic sections from brains were prefixed with paraformaldehyde during 24h and incubated in 30% sucrose (Fisher Scientific) 24H at 4°C. Brains were embedded in OCT, frozen at -80°C and stored at -80°C. 30 µm-thick sections were cut with a cryostat (Leica CM3050 S, France), stored at 4°C in sodium phosphate buffer. Sections were processed as follows: Day 1: free-floating sections were rinsed in PBS, incubated for 20 min in PBS containing 0.3% Tween-20, and then rinsed three times for 10 min each in PBS. Slices were incubated 1h with 5% donkey serum in 0.3% PBS-T and then overnight or 72H at 4°C with the primary antibodies described in the antibodies section. Slides were rinsed three times for 10 min in 0.3% PBS-T and incubated for 60 min with secondary antibodies. Sections were rinsed

three times for 10 min in PBS before mounting. Tissues were observed on a confocal laser scanning microscope , TCS SP8X; with Leica software LAS X navigator, using a HC PL APO CS2 20x /0.75 dry leica objective. The objectives and the pinhole setting (1 airy unit, au) remained unchanged during the acquisition of a series for all images. Quantification of immuno-positive cells was performed using the cell counter plugin of the ImageJ software taking as standard reference a fixed threshold of fluorescence.

Viral injections

Mice were anaesthetised with ketamine (130 mg per kg) and xylazine (13 mg per kg) and diluted in saline (5 µl per g of mouse) and placed into a stereotaxic apparatus (World Precision Instruments). For postoperative care, mice were injected intraperitoneally with buprenorphine (0,3 mg/kg). After exposing the skull via small incision, a small hole was drilled for injection. A Hamilton syringe connected to a 33G was inserted into the brain and virus was injected. A micromanipulator (World Precision Instruments) was used to control injection speed at 50 nl min−1 and the pipette was withdrawn 1 min after injection. For knockdown experiments, AAV8-SYN-LoxP-shRNA-CaMK1D-EGFP-LoxP or AAV8-SYN-LoxP-shRNA-Scramble-EGFP-LoxP (Universitat Autònoma de Barcelona; titer 1.12×10^{13} genome copies per ml) were bilaterally injected into the ARC (300 nl, AP: −1.40 mm, DV: −5.80 mm, ML: +/−0.10 mm from bregma). For rescue experiments, AAV2/9-CAGs-Flex-CaMK1Dwt-eGFP (IGBMC molecular biology and Virus Core; titer 2.7×10^{13} genome copies per ml) were bilaterally injected into the ARC (300 nl, coordinates as above). For CNO experiments, hSyn-DIO-hM3D(Gq)-mCherry (IGBMC molecular biology and Virus Core, titer 1.5×10^{13} genome copie per ml) were bilaterally injected into the ARC (300 nl, coordinates as above). Mice were given a minimum of 2 weeks recovery and 1 week acclimation before being used in any experiments.

Electrophysiology

Experiments were performed on brain slices from 9-12 week old male CaMK1D$^{+/+}$ and CaMK1D$^{-/-}$ mice that expressed enhanced green fluorescent protein (EGFP) selectively in AgRP neurons. Animals were kept under standard laboratory conditions, with tap water and chow available ad libitum, on a 12h light/dark cycle. The animals were lightly anesthetized with isoflurane (B506; AbbVie Deutschland GmbH and Co KG, Ludwigshafen, Germany) and decapitated. Coronal slices (280 µm) containing the arcuate nucleus of the hypothalamus were cut with a vibration microtome (VT1200 S; Leica, Germany) under cold (4°C), carbogenated (95% O2 and 5% CO2), glycerol-based modified artificial cerebrospinal fluid (GaCSF)[53].

Current-clamp recordings of GFP-expressing AgRP neurons were performed at ~32°C. Neurons were visualized with a fixed stage upright microscope (Zeiss AxioExaminer, Zeiss, Germany) using 40x water-immersion objective (W Plan-Apochromat 40x/1.0 DIC M27, 1 numerical aperture, 2.5 mm working distance; Zeiss) with infrared differential interference contrast optics[54] and fluorescence optics. GFP-expressing AgRP neurons were identified by their anatomical location in the arcuate nucleus and by their fluorescent label.

Perforated patch experiments were conducted using protocols modified from[55] and[56].

The spontaneous firing frequency was measured for 5 min after perforation. To measure intrinsic electrophysiological properties series of hyperpolarizing and depolarizing current pulses were applied under current clamp from a membrane potential of ~-70 mV. For input resistance and capacitance measurements, hyperpolarizing current steps with -2 pA increments were applied. For excitability measurements, depolarizing 1 s current steps with +2 pA increments were applied. The specific protocols are given in Results.

To investigate the modulatory effect of ghrelin (031-31, Phoenix Pharmaceuticals), 100 nM ghrelin was bath applied for 8-10 min. The ghrelin effect was analyzed by comparing the action potential frequencies that were measured during 2 min intervals that were recorded directly before and at the end of the peptide applications.

Data analysis of electrophysiological data

Data analysis was performed with Spike2 (version 7; Cambridge Electronic Design Ltd., Cambridge, UK), Igor Pro 6 (Wavemetrics, Portland, OR, USA), and Graphpad Prism 8. If not stated otherwise, all calculated values are expressed as means ± SEM (standard error of the mean). The horizontal lines show the data's median. The whiskers were calculated according to the 'Tukey' method. For comparisons of independent nonparametric distributions, the Mann-Whitney-U-test was used. Linear regressions were compared using the F-test. A significance level of 0.05 was accepted for all tests. Exact p-values are reported if $p > 0.05$. In the figures, n values are given in brackets.

Quantification and statistical analysis

All statistical comparisons were performed with Prism 6 (GraphPad Software, La Jolla, CA, USA) or R software for ANCOVA analysis. All the data were analyzed using either Student t test (paired or unpaired) with equal variances or One-way ANOVA or Two-way ANOVA. In all cases, significance threshold was automatically set at $p < 0.05$. ANOVA analyses were followed by Bonferroni post hoc test for specific comparisons only when overall ANOVA revealed a significant difference (at least $p < 0.05$).

Data Availability

Source data are provided with this paper. All raw data related to the studies shown in figures and extended data figures.

Acknowledgments

We thank T. Alquier at University of Montreal and D. Dembele at the IGBMC for helpful discussions. We thank the Imaging Center of the IGBMC (ICI), the IGBMC molecular biology and virus core facility, the Institut Clinique de la souris (ICS) core facilities and others core

facilities for their support on this research. This work was supported by the Agence Nationale de la Recherche (ANR) (AAPG 2017 LYSODIABETES and AAPG 2021 HypoCaMK)), by the Fondation de Recherche Médicale (FRM) – Program: Equipe FRM (EQU201903007859, Prix Roger PROPICE pour la recherche sur le cancer du pancréas), by the FHU-OMAGE of region Grand-Est, from the European Foundation for the Study of Diabetes (EFSD)/Novo Nordisk Diabetes Research Programme and by the ANR-10-LABX-0030-INRT grant as well as the ANR-11-INBS-0009-INGESTEM grant, both French State funds managed by the ANR under the frame program Investissements d'Avenir. K. Vivot was supported by an Individual Fellowship (798961 INSULYSOSOME) in the framework of the Marie-Sklodovska Curie actions of the European Commission and research grant from Société Francophone du Diabète. G. Yeghiazaryan received financial doctoral support from DFG-233886668/RTG1960. Ma. Quiñones was funded by a research contract Miguel Servet (CP21/00108) from the ISCIII co-funded by the European Union.

Author contributions

Conceptualization: R.R., R.P.N, P.K and S.L., Software: E.G., Methodology: K.V., E.P., Z.Z, Ma.Q, G.Y., E.E., E.C--C. and Me.Q, Validation: K.V., Formal Analysis: K.V., C.M., Investigation: K.V., G.M.,E.P., Z.Z., Ma.Q., E.E., G.Y., Me.Q., A.S., M.F and C.M., Resources: E.E.,F.B. Writing-Original Draft: R.R. and K.V., Supervision: K.V., S.L., P.K., R.P.R., A.C., I.S. and R.R, Funding Acquisition: R.R. and S.L.

Competing interests

All other authors declare no competing interests.

Figure legends

Figure 1. Global Deletion of *CaMK1D* gene reduces diet- and leptin deficiency-induced obesity in mice.

a, Expression of CaMK1D protein in different tissues from the wild type (*CaMK1D*$^{+/+}$) and whole-body *CaMK1D* knockout (*CaMK1D*$^{-/-}$) mice. **b**, Body weight of mice fed with a Chow diet (CD) (CD - *CaMK1D*$^{+/+}$ n = 9 ; CD - *CaMK1D*$^{-/-}$ n = 11) or a High Fat Diet (HFD) (HFD - *CaMK1D*$^{+/+}$ n = 11 ; HFD - *CaMK1D*$^{-/-}$ n = 11). **c**, Body composition of mice fed with a HFD measured by qNMR. (n=9/ group) (FBF = free body fluid). **d**, Body weight of leptin deficient mice (*ob/ob* mice) fed with a Chow diet (CD). (n = 7/group). **e**, 4 hours fasted blood glucose levels. (CD - *CaMK1D*$^{+/+}$ n = 8 ; CD - *CaMK1D*$^{-/-}$ n = 9 ; HFD - *CaMK1D*$^{+/+}$ n = 8 ; HFD - *CaMK1D*$^{-/-}$ n = 9). **f**, 4 hours fasted plasma insulin levels. (CD - *CaMK1D*$^{+/+}$ n = 9 ; CD - *CaMK1D*$^{-/-}$ n = 10 ; HFD - *CaMK1D*$^{+/+}$ n = 10 ; HFD - *CaMK1D*$^{-/-}$ n = 9). **g-i**, Blood glucose levels during an IPGTT in mice with the indicated genotypes and diets. Corresponding areas Under the Curve (AUC) are depicted. (CD - *CaMK1D*$^{+/+}$ n = 9 ; CD - *CaMK1D*$^{-/-}$ n = 11 ; HFD - *CaMK1D*$^{+/+}$ n = 11 ; HFD - *CaMK1D*$^{-/-}$ n = 12). **j-l**, Blood glucose levels during ITT in mice with the indicated genotypes and diets. kITTs obtained from ITT are depicted. (CD - *CaMK1D*$^{+/+}$ n = 10; CD - *CaMK1D*$^{-/-}$ n = 10 ; HFD - *CaMK1D*$^{+/+}$ n = 7 ; HFD - *CaMK1D*$^{-/-}$ n = 7). Data are presented as mean values +/- SEM. $*p < 0.05$ and $**p < 0.01$. Statistical tests included two-way ANOVA bonferroni post hoc test (**b**, **c, d, e, f, h**, **k**) and unpaired Student's t test (**i**, **l**).

Figure 2. Deletion of *CaMK1D* attenuates ghrelin-induced food intake. a-b, Cumulative food intake from mice. (CD - *CaMK1D*$^{+/+}$ n = 9; CD - *CaMK1D*$^{-/-}$ n = 11 ; HFD - *CaMK1D*$^{+/+}$ n = 9 ; HFD - *CaMK1D*$^{-/-}$ n = 10). **c**, Cumulative food intake of leptin deficient mice (*ob/ob* mice) fed with a chow diet (*CaMK1D*$^{+/+}$ n = 7 ; HFD - *CaMK1D*$^{-/-}$ n = 8). **d**, Cumulative food intake from mice on a HFD. Food intake was determined 24H after food withdrawal. (*CaMK1D*$^{+/+}$ n = 12 ; HFD - *CaMK1D*$^{-/-}$ n = 17). **e**, Regression-based analysis of absolute MR against body weight in HFD fed control (*CaMK1D*$^{+/+}$) and whole body *CaMK1D* knockout (*CaMK1D*$^{-/-}$) mice (*CaMK1D*$^{+/+}$ n = 7 ; HFD - *CaMK1D*$^{-/-}$ n = 9). The ANCOVA analysis was done with MR as a dependent variable, the genotype as a fixed variable and body mass as a covariate. **f-g**, Ambulatory

activity over 24H. Ambulatory activity was measured with mice deprived from food for 24H. AUC from 5PM to 11PM was calculated (n=6 / group). **h**, Cumulative food intake after ghrelin injections (30 µg / day) of mice on a chow diet. (*CaMK1D*$^{+/+}$ n = 6 ; *CaMK1D*$^{-/-}$ n = 7) **i**, Cumulative food intake after leptin injections (3mg / kg) of mice on a chow diet. Food intake was determined 24H after food withdrawal. (*CaMK1D*$^{+/+}$ n = 6 ; *CaMK1D*$^{-/-}$ n = 7). **j**, Blood acylated Ghrelin (*CaMK1D*$^{+/+}$ n = 8 ; HFD - *CaMK1D*$^{-/-}$ n = 5) and **k**, Blood Leptin (N= 6 / group) levels in mice on a HFD. Blood sampling was performed 4H after food withdrawal. Data are presented as mean values +/- SEM. $*p < 0.05$ and $**p < 0.01$. Statistical tests included two-way ANOVA bonferroni post hoc test (**a**,**b**,**c**,**d**,**h**,**i**), ANCOVA (**e**) and unpaired Student's t test (**g**,**j**,**k**).

Figure 3. CaMK1D deletion in AgRP neurons leads to reduced body weight and food intake. **a**, Body weight of mice on a Chow diet (CD) or on a High Fat Diet (HFD) (*CaMK1D*$^{flox/flox}$: CD n = 15 / HFD n = 15; *AgRP*$^{Cre/+}$ CD n = 14 / HFD n = 11; *AgRP*$^{Cre/+}$; *CaMK1D*$^{flox/flox}$ CD n=16 / HFD n= 13). **b-c,** Cumulative food intake fed on CD or a HFD (*CaMK1D*$^{flox/flox}$: CD n = 15 / HFD n = 15; *AgRP*$^{Cre/+}$ CD n = 14 / HFD n = 11; *AgRP*$^{Cre/+}$; *CaMK1D*$^{flox/flox}$ CD n=15 / HFD n= 12). **d**, Cumulative food intake after 24h fasting. (*CaMK1D*$^{flox/flox}$ n = 8 ; *AgRP*$^{Cre/+}$ n = 9 and *AgRP*$^{Cre/+}$; *CaMK1D*$^{flox/flox}$ n=7). **e**, Cumulative food intake after ghrelin injections. (*CaMK1D*$^{flox/flox}$ n = 10 ; *AgRP*$^{Cre/+}$ n = 9 ; *AgRP*$^{Cre/+}$; *CaMK1D*$^{flox/flox}$ n=9). **f**, Microscopy picture of Nuclei (DAPI), AgRP neurons (red), viral eGFP (green) and merge (Yellow). **g**, Cumulative food intake after ghrelin injections. (AAV DIO scramble eGFP n = 13 ; AAV DIO shCAMK1D eGFP n = 10). **h**, Microscopy picture of Nuclei (DAPI), AgRP neurons (red), viral eGFP (green) and Merge (yellow): Arcuate nucleus, 3V : third ventricule **i**, Cumulative food intake after ghrelin injections and before AAVs injection. (n = 8 / group). **j**, Expression of *CaMK1D* mRNA (*AgRP*$^{Cre/+}$: AAV eGFP n=5 / AAV *CaMK1D* eGFP n=5; *AgRP*$^{Cre/+}$; *CaMK1D*$^{flox/flox}$: AAV eGFP n = 7/ AAV *CaMK1D* eGFP n = 9). **k**, Cumulative food intake after ghrelin injections and after AAVs injection. (*AgRP*$^{Cre/+}$: AAV eGFP n=6 / AAV *CaMK1D* eGFP n=14; *AgRP*$^{Cre/+}$;

CaMK1D$^{flox/flox}$: AAV eGFP n = 8/ AAV *CaMK1D* eGFP n = 15). **l**, Microscopy picture of Nuclei (DAPI), AgRP neurons (green), mCherry (red) and Merge (Yellow). **m**, Cumulative food intake after CNO injections of mice before AAVs injection (*AgRP*$^{Cre/+}$ n = 8 ; *AgRP*$^{Cre/+}$; *CaMK1D*$^{flox/flox}$ n=11). **n**, Cumulative food intake after CNO injections and after AAVs injection. (*AgRP*$^{Cre/+}$ n = 7 and *AgRP*$^{Cre/+}$; *CaMK1D*$^{flox/flox}$ n=8). Data are presented as mean values +/- SEM. $*p < 0.05$, $**p< 0.01$ and $***p < 0.001$. Statistical tests included two-way ANOVA bonferroni post hoc test (**a**,**b**,**c**,**d**,**e**,**g**,**i**,**j**,**k**,**m**,**n**).

Figure 4. Conditional deletion of *CaMK1D* in AgRP neurons decreases energy expenditure.

a, Cumulative food intake on a Chow Diet (CD). Food intake was determined 48h during indirect calorimetric measurements. (*CaMK1D*$^{flox/flox}$ n = 9 ; *AgRP*$^{Cre/+}$ n = 10 and *AgRP*$^{Cre/+}$; *CaMK1D*$^{flox/flox}$ n=9). **b-c**, Locomotor activity over 48h on a CD. *(CaMK1D*$^{flox/flox}$ n = 9 ; *AgRP*$^{Cre/+}$ n = 9 and *AgRP*$^{Cre/+}$; *CaMK1D*$^{flox/flox}$ n=9) **d**, Regression-based analysis of absolute MR against body weight in of mice on a CD. The ANCOVA analysis was done with MR as a dependent variable, the genotype as a fixed variable and body mass as a covariate. All indirect calorimetric measurements were done in automated cages. (*CaMK1D*$^{flox/flox}$ n = 7 ; *AgRP*$^{Cre/+}$ n = 8 and *AgRP*$^{Cre/+}$; *CaMK1D*$^{flox/flox}$ n=9). Data are presented as mean values +/- SEM. Statistical tests included ANCOVA (**d**).

Figure 5. CaMK1D is dispensable for ghrelin-induced electrophysiological activation of AgRP/NPY neurons

a-b, Representative immunofluorescence and quantification of NPY-GFP^{+} and c-fos^{+} cells in the ARC of mice. Animals were injected with 30 µg ghrelin or vehicle and 2h after injections whole hypothalamus was removed. (Sal - *CaMK1D*$^{+/+}$ n = 5 ; Ghl - *CaMK1D*$^{+/+}$ n = 5 ; Sal - *CaMK1D*$^{-/-}$ n = 3 ; Ghl - *CaMK1D*$^{-/-}$ n=4) **c**, Recording situation shown in a brightfield (top) and fluorescent

image (bottom). The AgRP neuron expressed EGFP (green) and the recording pipette contained tetramethyl rhodamine dextrane (red) to monitor membrane integrity during the perforated patch clamp recording. **d**, Recording of an AgRP neuron from a *CaMK1D*$^{+/+}$ mouse during ghrelin (100 nM) bath application. Top: Rate histogram, bin width: 10 s. Middle: Original recording. Bottom: Segments of the original recording in higher time resolution. The numbers indicate the time points from which the segments originate. **e**, Ghrelin responses of AgRP neurons from *CaMK1D*$^{+/+}$ and in *CaMK1D*$^{-/-}$ mice, expressed as change in action potential frequency. Top: Mean (± SEM) responses during the first 5 min of ghrelin application. Bottom: Box plots showing the change in action potenial frequency measured between 6 and 8 min of ghrelin application. **f-i**, Basic electrophysiological properties of AgRP neurons in *CaMK1D*$^{+/+}$ and in *CaMK1D*$^{-/-}$ mice. **f**, Spontaneous action potential frequency. **g**, Excitability assessed by the number of action potentials (APs) as a function of current pulse (1s) amplitude. **h**, Input resistance. **i**, Whole-cell capacitance. The horizontal lines in the box plots show the median. The whiskers were calculated according to the 'Tukey' method. ∗∗∗$p < 0.001$. Statistical tests included unpaired Student's t test (**a**). Data in (**e**,**f**,**h**,and **i**) were compared using the Mann-Whitney-U-test, and linear regressions in (**g**) were compared using the F-test. n values are given in brackets. Data are presented as mean values +/- SEM

Figure 6. Lack of CaMK1D reduces ghrelin-induced AgRP/NPY expression and abundance in AgRP neuron projections to the PVN. a, Representative Phos-tag immunoblot of CaMK1D using lysates of hypothalamic cells from mice treated with 1 µM Ghrelin or vehicle for 5 min. **b**, Representative immunoblot of pS179/T180 CaMK1D using lysates of whole hypothalamus from mice with indicated genotypes. Animals were injected with 30 µg ghrelin or vehicle and 2h after injections whole hypothalamus was removed and used for protein extraction.. **c**, Quantification of CAMK1D phosphorylation (N=4/group). **d**, Representative immunoblots of pS79-ACC and pT172-AMPK using lysates of hypothalamic primary neurons from mice with indicated genotypes

treated with 1 µM Ghrelin or vehicle for 5 min. **e-f**, Quantification of ACC (N=4/group) and AMPK phosphorylation (N=3/group). **g**, Representative Immunofluoresence of pS133 CREB using hypothalamic slices of NPY-GFP mice with indicated genotypes. Animals were injected with 30 µg ghrelin or vehicle and 2h after injections whole brain containing hypothalamus was removed, Nuclei stained with DAPI, pS133 CREB (red), NPY-GFP (green). PVN : paraventricular nucleus, 3V : third ventricule. **h**, Quantification of pS133 CREB fluorescence intensity in NPY-GFP^{+} neurons (N=4/group). **i**, Expression of AgRP, NPY and POMC mRNA in whole hypothalamus. Animals were injected with 30 µg ghrelin or vehicle and whole hypothalamus was removed 2H after injections. (*CaMK1D*$^{+/+}$ n = 6 ; *CaMK1D*$^{+/+}$ n = 5). **j-m,** Representative immunofluorescence and quantification of AgRP (Sal - *CaMK1D*$^{+/+}$ n = 7 ; Ghl - *CaMK1D*$^{+/+}$ n = 6 ; Sal - *CaMK1D*$^{-/-}$ n = 6 ; Ghl - *CaMK1D*$^{-/-}$ n = 6) and NPY (*CaMK1D*$^{+/+}$ n = 5 ; *CaMK1D*$^{-/-}$ n = 5) projections to the PVN. Animals were injected with 30 µg ghrelin and 2h after injections, brain was removed. **g**, Schematic model depicting mechanisms how CaMK1D promotes food intake. Data are presented as mean values +/- SEM. $*p < 0.05$ and $***p < 0.001$. Statistical tests included unpaired Student's t test (**c**,**e**,**f**,**h**,**i**,**k**,**m**).

Extended Data Figure 1. Deletion of *CaMK1D* in mice does not affect body size and *CaMK1D* knockout mice are born without any gross abnormalities. a, Schematic screen of targeting of the CaMK1D locus using Knockout-first targeting strategy and generation of floxed and global knockout mice. For further details see material and methods. **b**, Validation of targeted ES clone by southern blot. Genomic DNA was digested using BspHI, BstEII, ApaII or EcoRI. The table shows the expected size of bands corresponding to the restriction enzyme used. A probe recognizing the neoR cassette was used. **c**, Gender distribution of mice and **d**, Mendelian ratios of born mice with indicated genetoypes. **e**, Body length and **f**, Tibia Length measurements of 7-week-old mice with

indicated genotypes (*CaMK1D*$^{+/+}$ n = 5 ; *CaMK1D*$^{-/-}$ n = 7). Data are presented as mean values +/- SEM.

Extended Data Figure 2. CaMK1D signaling is redundant in pancreatic beta cell and liver function.

a, Blood insulin levels during IPGTTs in mice on a High fat diet (HFD). (n=11/group). **b**, Glucose-stimulated insulin secretion (GSIS) in pancreatic islets isolated from mice. (*CaMK1D*$^{+/+}$ n = 6 ; *CaMK1D*$^{-/-}$ n = 5). **c**, Expression of CaMK1D protein in pancreas and brain from mice with indicated genotypes. **d**, Body weight gain of mice on a Chow diet (CD) or on a High Fat Diet (HFD). (CD - *CaMK1D*$^{flox/flox}$ n = 13 ; CD - *AgRP*$^{Cre/+}$; *CaMK1D*$^{flox/flox}$ n= 13 ; HFD - *CaMK1D*$^{flox/flox}$ n = 12 ; CD - *AgRP*$^{Cre/+}$; *CaMK1D*$^{flox/flox}$ n= 10). **e-f**, Blood glucose levels during IPGTTs in mice on a CD (**e**), or on a HFD (**f**). (CD - *CaMK1D*$^{flox/flox}$ n = 7 ; CD - *AgRP*$^{Cre/+}$; *CaMK1D*$^{flox/flox}$ n= 6 ; HFD - *CaMK1D*$^{flox/flox}$ n = 7 ; CD - *AgRP*$^{Cre/+}$; *CaMK1D*$^{flox/flox}$ n= 8).
g, Expression of CaMK1D mRNA in liver from mice. (*CaMK1D*$^{flox/flox}$ n = 3 ; CD - *Alb*$^{Cre/+}$; *CaMK1D*$^{flox/flox}$ n= 3) **h**, Body weight gain of mice on a CD or on a HFD. (CD - *CaMK1D*$^{flox/flox}$ n = 8 ; CD - *Alb*$^{Cre/+}$; *CaMK1D*$^{flox/flox}$ n= 9; HFD - *CaMK1D*$^{flox/flox}$ n = 8 ; HFD - *Alb*$^{Cre/+}$; *CaMK1D*$^{flox/flox}$ n= 10). Blood glucose levels during an IPGTT in mice on a CD (**i**) or on a HFD (**j**). (CD - *CaMK1D*$^{flox/flox}$ n = 6 ; CD - *Alb*$^{Cre/+}$; *CaMK1D*$^{flox/flox}$ n= 7; HFD - *CaMK1D*$^{flox/flox}$ n = 8 ; HFD - *Alb*$^{Cre/+}$; *CaMK1D*$^{flox/flox}$ n= 5). Blood glucose levels during an ITT in mice on a CD (**k**) or on a HFD (**l**). (CD - *CaMK1D*$^{flox/flox}$ n = 5 ; CD - *Alb*$^{Cre/+}$; *CaMK1D*$^{flox/flox}$ n= 6; HFD - *CaMK1D*$^{flox/flox}$ n = 12 ; HFD - *Alb*$^{Cre/+}$; *CaMK1D*$^{flox/flox}$ n= 14). Data are presented as mean values +/- SEM.

Extended Data Figure 3. Deletion of *CaMK1D* does not result in anxiety-like behavior and stress-induced anhedonia. a,Distance traveled each 5 min, and (**b**) in total. (**c**) Rear number

each 5 min, and (**d**) in total. **e**, Number of entries in the center or periphery of the arena. **f**, Time spent in the center or periphery of the arena. **g**, Average speed during an open field test. (n=8/group). **h**, Amount of sucrose and water consumed over 3 day in while sucrose and water were both available in the same time. (*CaMK1D*$^{+/+}$ n = 8 ; *CaMK1D*$^{-/-}$ n = 7). Data are presented as mean values +/- SEM.

Extended Data Figure 4. Deletion of *CaMK1D* in the Nervous Tissue reproduces phenotypes in whole-body knockout mice. a, Expression of CaMK1D protein in mice. **b**, Body weight gain on a Chow diet (CD) or on a High Fat Diet (HFD). (CD - *CaMK1D*$^{flox/flox}$ n = 12 ; CD - *Nestin*$^{Cre/+}$ n = 11 and CD - *Nestin*$^{Cre/+}$; *CaMK1D*$^{flox/flox}$ n= 10 ; HFD - *CaMK1D*$^{flox/flox}$ n = 12 ; HFD - *Nestin*$^{Cre/+}$ n = 12 HFD - *Nestin*$^{Cre/+}$; *CaMK1D*$^{flox/flox}$ n= 11). Cumulative food intake on (**c**) CD or on (**d**) HFD. (CD - *CaMK1D*$^{flox/flox}$ n = 12 ; CD - *Nestin*$^{Cre/+}$ n = 11 and CD - *Nestin*$^{Cre/+}$; *CaMK1D*$^{flox/flox}$ n= 10 ; HFD - *CaMK1D*$^{flox/flox}$ n = 12 ; HFD - *Nestin*$^{Cre/+}$ n = 12 HFD - *Nestin*$^{Cre/+}$; *CaMK1D*$^{flox/flox}$ n= 11) (*p ≤ 0.05). (**e**) Cumulative food intake. (*CaMK1D*$^{flox/flox}$ n = 10 ; *Nestin*$^{Cre/+}$ n = 12 and *Nestin*$^{Cre/+}$; *CaMK1D*$^{flox/flox}$ n= 8). (**f**) Cumulative food intake after ghrelin injection (30 µg / day) on a CD. (*CaMK1D*$^{flox/flox}$ n = 7 ; *Nestin*$^{Cre/+}$ n = 10 and *Nestin*$^{Cre/+}$; *CaMK1D*$^{flox/flox}$ n= 9). Data are presented as mean values +/- SEM. ∗p < 0.05, ∗∗p< 0.01 and ∗∗∗p < 0.001. Statistical tests included two-way ANOVA bonferroni post hoc test (**b**,**c**,**d,e,f**).

Extended Data Figure 5. Deletion of *CaMK1D* in AgRP neurons. a, Verification of recombination in the CaMK1D locus in hypothalamus (Hyp), cortex (Crtx), liver, tail and white blood cells (WBC) from mice. **b**, Expression of *CaMK1D* mRNA in arcuate nucleus, cortex and liver from mice (n=4 / group).Statistical tests included unpaired t-test (**b**). Data are presented as mean values +/- SEM.

Extended Data Figure 6. Deletion of *CaMK1D* in POMC neurons does not affect energy metabolism in mice. a, Verification of recombination in the CaMK1D locus in hypothalamus (Hyp), cortex (Crtx), liver, tail and white blood cells (WBC) from mice. **b**, Body weight gain on a Chow diet (CD) or on a High Fat Diet (HFD). (CD - $CaMK1D^{flox/flox}$ n = 11 ; CD -$POMC^{Cre/+}$ n = 8 ; CD -$POMC^{Cre/+}$; $CaMK1D^{flox/flox}$ n= 8; HFD - $CaMK1D^{flox/flox}$ n = 10 ; HFD -$POMC^{Cre/+}$ n = 10 and HFD -$POMC^{Cre/+}$; $CaMK1D^{flox/flox}$ n= 13).**c**, Cumulative food intake on a CD. (CD - $CaMK1D^{flox/flox}$ n = 10 ; CD -$POMC^{Cre/+}$ n = 8 ; CD -$POMC^{Cre/+}$; $CaMK1D^{flox/flox}$ n= 8). **d**, Cumulative food intake on a HFD. (HFD - $CaMK1D^{flox/flox}$ n = 10 ; HFD -$POMC^{Cre/+}$ n = 8 ; HFD -$POMC^{Cre/+}$; $CaMK1D^{flox/flox}$ n= 10). **e**, Cumulative food intake. Food intake was determined 24h after fasting. ($CaMK1D^{flox/flox}$ n = 10 ; $POMC^{Cre/+}$ n = 8 ; $POMC^{Cre/+}$; $CaMK1D^{flox/flox}$ n= 10). **f**, Cumulative food intake after ghrelin injection. ($CaMK1D^{flox/flox}$ n = 8 ; $POMC^{Cre/+}$ n = 7 ; $POMC^{Cre/+}$; $CaMK1D^{flox/flox}$ n= 8). Data are presented as mean values +/- SEM. $**p< 0.01$ and $***p < 0.001$. Statistical tests included two-way ANOVA bonferroni post hoc test (**f**).

Extended Data Table 1. **List of reagents and other resources used in this study.** Antibodies, Chemicals, Peptides, Recombinant proteins, Critical Commercial assays, Mouse Lines, Software and Algorithms and Primers are listed in the table according to their supplier and identifier.

References

1. Kim, K.-S., Seeley, R. J. & Sandoval, D. A. Signalling from the periphery to the brain that regulates energy homeostasis. *Nat. Rev. Neurosci.* **19**, 185–196 (2018).
2. Jais, A. & Brüning, J. C. Arcuate nucleus-dependent regulation of metabolism - pathways to obesity and diabetes mellitus. *Endocr Rev* bnab025 (2021) doi:10.1210/endrev/bnab025.
3. Morton, G. J., Cummings, D. E., Baskin, D. G., Barsh, G. S. & Schwartz, M. W. Central nervous system control of food intake and body weight. *Nature* **443**, 289–295 (2006).
4. Timper, K. & Brüning, J. C. Hypothalamic circuits regulating appetite and energy homeostasis: pathways to obesity. *Dis Model Mech* **10**, 679–689 (2017).
5. Chen, S.-R. *et al.* Ghrelin receptors mediate ghrelin-induced excitation of agouti-related protein/neuropeptide Y but not pro-opiomelanocortin neurons. *J. Neurochem.* **142**, 512–520 (2017).
6. Zigman, J. M., Bouret, S. G. & Andrews, Z. B. Obesity Impairs the Action of the

Neuroendocrine Ghrelin System. *Trends Endocrinol Metab* **27**, 54–63 (2016).
7. Bonnefond, A. & Froguel, P. Rare and common genetic events in type 2 diabetes: what should biologists know? *Cell Metab.* **21**, 357–368 (2015).
8. Locke, A. E. *et al.* Genetic studies of body mass index yield new insights for obesity biology. *Nature* **518**, 197–206 (2015).
9. Kooner, J. S. *et al.* Genome-wide association study in individuals of South Asian ancestry identifies six new type 2 diabetes susceptibility loci. *Nat. Genet.* **43**, 984–989 (2011).
10. Shu, X. O. *et al.* Identification of new genetic risk variants for type 2 diabetes. *PLoS Genet.* **6**, e1001127 (2010).
11. Zeggini, E. *et al.* Meta-analysis of genome-wide association data and large-scale replication identifies additional susceptibility loci for type 2 diabetes. *Nature genetics* **40**, 638–45 (2008).
12. Morris, A. P. *et al.* Large-scale association analysis provides insights into the genetic architecture and pathophysiology of type 2 diabetes. *Nat. Genet.* **44**, 981–990 (2012).
13. Thurner, M. *et al.* Integration of human pancreatic islet genomic data refines regulatory mechanisms at Type 2 Diabetes susceptibility loci. *Elife* **7**, (2018).
14. Xue, A. *et al.* Genome-wide association analyses identify 143 risk variants and putative regulatory mechanisms for type 2 diabetes. *Nat Commun* **9**, 2941 (2018).
15. Simonis-Bik, A. M. *et al.* Gene variants in the novel type 2 diabetes loci CDC123/CAMK1D, THADA, ADAMTS9, BCL11A, and MTNR1B affect different aspects of pancreatic beta-cell function. *Diabetes* **59**, 293–301 (2010).
16. Haney, S. *et al.* RNAi screening in primary human hepatocytes of genes implicated in genome-wide association studies for roles in type 2 diabetes identifies roles for CAMK1D and CDKAL1, among others, in hepatic glucose regulation. *PLoS ONE* **8**, e64946 (2013).
17. Buchser, W. J., Slepak, T. I., Gutierrez-Arenas, O., Bixby, J. L. & Lemmon, V. P. Kinase/phosphatase overexpression reveals pathways regulating hippocampal neuron morphology. *Mol. Syst. Biol.* **6**, 391 (2010).
18. Wayman, G. A. *et al.* Regulation of axonal extension and growth cone motility by calmodulin-dependent protein kinase I. *J. Neurosci.* **24**, 3786–3794 (2004).
19. Takemoto-Kimura, S. *et al.* Regulation of dendritogenesis via a lipid-raft-associated Ca2+/calmodulin-dependent protein kinase CLICK-III/CaMKIgamma. *Neuron* **54**, 755–770 (2007).
20. Schmitt, J. M., Guire, E. S., Saneyoshi, T. & Soderling, T. R. Calmodulin-dependent kinase kinase/calmodulin kinase I activity gates extracellular-regulated kinase-dependent long-term potentiation. *J. Neurosci.* **25**, 1281–1290 (2005).
21. Soriano, P. Generalized lacZ expression with the ROSA26 Cre reporter strain. *Nat Genet* **21**, 70–71 (1999).
22. Gu, G., Dubauskaite, J. & Melton, D. A. Direct evidence for the pancreatic lineage: NGN3+ cells are islet progenitors and are distinct from duct progenitors. *Development* **129**, 2447–2457 (2002).
23. Hatting, M., Tavares, C. D. J., Sharabi, K., Rines, A. K. & Puigserver, P. Insulin regulation of gluconeogenesis. *Ann N Y Acad Sci* **1411**, 21–35 (2018).
24. Postic, C. *et al.* Dual roles for glucokinase in glucose homeostasis as determined by liver and pancreatic beta cell-specific gene knock-outs using Cre recombinase. *J Biol Chem* **274**, 305–315 (1999).
25. Müller, T. D. *et al.* Ghrelin. *Mol Metab* **4**, 437–460 (2015).
26. Andrews, Z. B. *et al.* UCP2 mediates ghrelin's action on NPY/AgRP neurons by lowering free radicals. *Nature* **454**, 846–851 (2008).
27. Hoffman, G. E., Smith, M. S. & Verbalis, J. G. c-Fos and related immediate early

gene products as markers of activity in neuroendocrine systems. *Front Neuroendocrinol* **14**, 173–213 (1993).
28. van den Pol, A. N. *et al.* Neuromedin B and gastrin-releasing peptide excite arcuate nucleus neuropeptide Y neurons in a novel transgenic mouse expressing strong Renilla green fluorescent protein in NPY neurons. *J Neurosci* **29**, 4622–4639 (2009).
29. Haribabu, B. *et al.* Human calcium-calmodulin dependent protein kinase I: cDNA cloning, domain structure and activation by phosphorylation at threonine-177 by calcium-calmodulin dependent protein kinase I kinase. *EMBO J* **14**, 3679–3686 (1995).
30. Andersson, U. *et al.* AMP-activated protein kinase plays a role in the control of food intake. *J Biol Chem* **279**, 12005–12008 (2004).
31. Sakkou, M. *et al.* A role for brain-specific homeobox factor Bsx in the control of hyperphagia and locomotory behavior. *Cell Metab* **5**, 450–463 (2007).
32. Sheng, M., Thompson, M. A. & Greenberg, M. E. CREB: a Ca(2+)-regulated transcription factor phosphorylated by calmodulin-dependent kinases. *Science* **252**, 1427–1430 (1991).
33. Flavell, S. W. & Greenberg, M. E. Signaling mechanisms linking neuronal activity to gene expression and plasticity of the nervous system. *Annu Rev Neurosci* **31**, 563–590 (2008).
34. Aponte, Y., Atasoy, D. & Sternson, S. M. AGRP neurons are sufficient to orchestrate feeding behavior rapidly and without training. *Nat Neurosci* **14**, 351–355 (2011).
35. Chen, H. Y. *et al.* Orexigenic action of peripheral ghrelin is mediated by neuropeptide Y and agouti-related protein. *Endocrinology* **145**, 2607–2612 (2004).
36. Luquet, S., Perez, F. A., Hnasko, T. S. & Palmiter, R. D. NPY/AgRP neurons are essential for feeding in adult mice but can be ablated in neonates. *Science* **310**, 683–685 (2005).
37. Nakazato, M. *et al.* A role for ghrelin in the central regulation of feeding. *Nature* **409**, 194–198 (2001).
38. Wu, C.-S. *et al.* Suppression of GHS-R in AgRP Neurons Mitigates Diet-Induced Obesity by Activating Thermogenesis. *Int J Mol Sci* **18**, 832 (2017).
39. Wang, Q. *et al.* Arcuate AgRP neurons mediate orexigenic and glucoregulatory actions of ghrelin. *Mol Metab* **3**, 64–72 (2014).
40. Anderson, K. A. *et al.* Hypothalamic CaMKK2 contributes to the regulation of energy balance. *Cell Metab.* **7**, 377–388 (2008).
41. López, M. *et al.* Hypothalamic fatty acid metabolism mediates the orexigenic action of ghrelin. *Cell Metab* **7**, 389–399 (2008).
42. García, A., Alvarez, C. V., Smith, R. G. & Diéguez, C. Regulation of Pit-1 expression by ghrelin and GHRP-6 through the GH secretagogue receptor. *Mol Endocrinol* **15**, 1484–1495 (2001).
43. Gonzalez, G. A. & Montminy, M. R. Cyclic AMP stimulates somatostatin gene transcription by phosphorylation of CREB at serine 133. *Cell* **59**, 675–680 (1989).
44. Kohno, D., Gao, H.-Z., Muroya, S., Kikuyama, S. & Yada, T. Ghrelin directly interacts with neuropeptide-Y-containing neurons in the rat arcuate nucleus: Ca2+ signaling via protein kinase A and N-type channel-dependent mechanisms and cross-talk with leptin and orexin. *Diabetes* **52**, 948–956 (2003).
45. Martins, L. *et al.* Hypothalamic mTOR signaling mediates the orexigenic action of ghrelin. *PLoS One* **7**, e46923 (2012).
46. Stevanovic, D. *et al.* Ghrelin-induced food intake and adiposity depend on central mTORC1/S6K1 signaling. *Mol Cell Endocrinol* **381**, 280–290 (2013).
47. Albert, V., Cornu, M. & Hall, M. N. mTORC1 signaling in Agrp neurons mediates circadian expression of Agrp and NPY but is dispensable for regulation of feeding behavior.

Biochem Biophys Res Commun **464**, 480–486 (2015).
48. Codner, G. F. *et al.* Universal Southern blot protocol with cold or radioactive probes for the validation of alleles obtained by homologous recombination. *Methods* **191**, 59–67 (2021).
49. Lundbaek, K. Intravenous glucose tolerance as a tool in definition and diagnosis of diabetes mellitus. *Br Med J* **1**, 1507–1513 (1962).
50. Even, P. C. & Nadkarni, N. A. Indirect calorimetry in laboratory mice and rats: principles, practical considerations, interpretation and perspectives. *Am J Physiol Regul Integr Comp Physiol* **303**, R459-476 (2012).
51. Müller, T. D., Klingenspor, M. & Tschöp, M. H. Revisiting energy expenditure: how to correct mouse metabolic rate for body mass. *Nat Metab* **3**, 1134–1136 (2021).
52. Pfaffl, M. W. A new mathematical model for relative quantification in real-time RT-PCR. *Nucleic Acids Res* **29**, e45 (2001).
53. Ye, J. H., Zhang, J., Xiao, C. & Kong, J.-Q. Patch-clamp studies in the CNS illustrate a simple new method for obtaining viable neurons in rat brain slices: glycerol replacement of NaCl protects CNS neurons. *J Neurosci Methods* **158**, 251–259 (2006).
54. Dodt, H. U. & Zieglgänsberger, W. Visualizing unstained neurons in living brain slices by infrared DIC-videomicroscopy. *Brain Res* **537**, 333–336 (1990).
55. Horn, R. & Marty, A. Muscarinic activation of ionic currents measured by a new whole-cell recording method. *J Gen Physiol* **92**, 145–159 (1988).
56. Akaike, N. & Harata, N. Nystatin perforated patch recording and its applications to analyses of intracellular mechanisms. *Jpn J Physiol* **44**, 433–473 (1994).

Figure 1

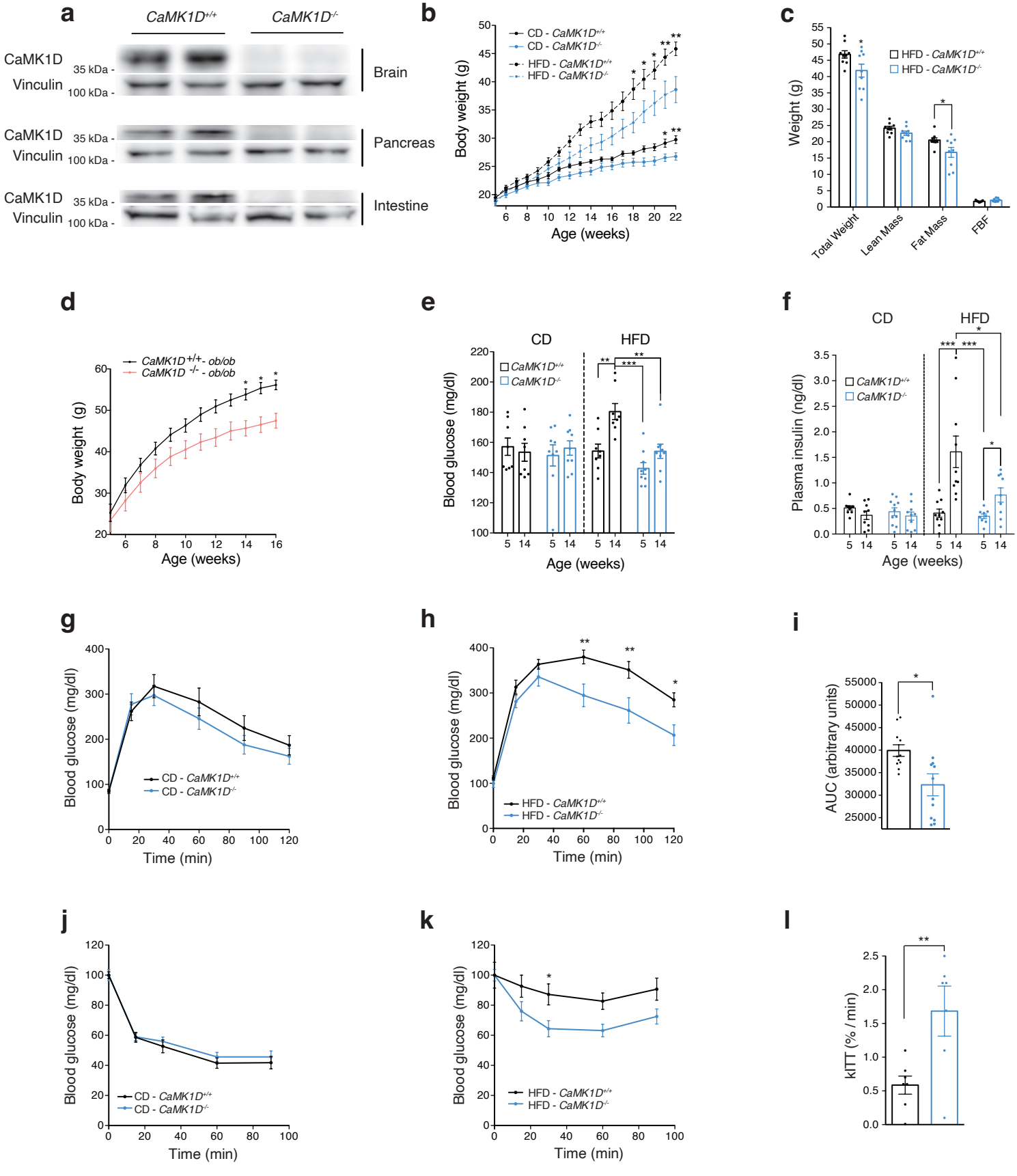
a
CaMK1D+/+
CaMK1D-/-
CaMK1D
Vinculin
35 kDa -
100 kDa -
Brain
Pancreas
Intestine
b
CD - CaMK1D+/+
CD - CaMK1D-/-
HFD - CaMK1D+/+
HFD - CaMK1D-/-
Body weight (g)
Age (weeks)
c
HFD - CaMK1D+/+
HFD - CaMK1D-/-
Weight (g)
Total Weight
Lean Mass
Fat Mass
FBF
d
CaMK1D+/+ - ob/ob
CaMK1D -/- - ob/ob
Body weight (g)
Age (weeks)
e
CD
HFD
CaMK1D+/+
CaMK1D-/-
Blood glucose (mg/dl)
Age (weeks)
f
CD
HFD
CaMK1D+/+
CaMK1D-/-
Plasma insulin (ng/dl)
Age (weeks)
g
CD - CaMK1D+/+
CD - CaMK1D-/-
Blood glucose (mg/dl)
Time (min)
h
HFD - CaMK1D+/+
HFD - CaMK1D-/-
Blood glucose (mg/dl)
Time (min)
i
AUC (arbitrary units)
j
CD - CaMK1D+/+
CD - CaMK1D-/-
Blood glucose (mg/dl)
Time (min)
k
HFD - CaMK1D+/+
HFD - CaMK1D-/-
Blood glucose (mg/dl)
Time (min)
l
kITT (% / min)

Figure 2

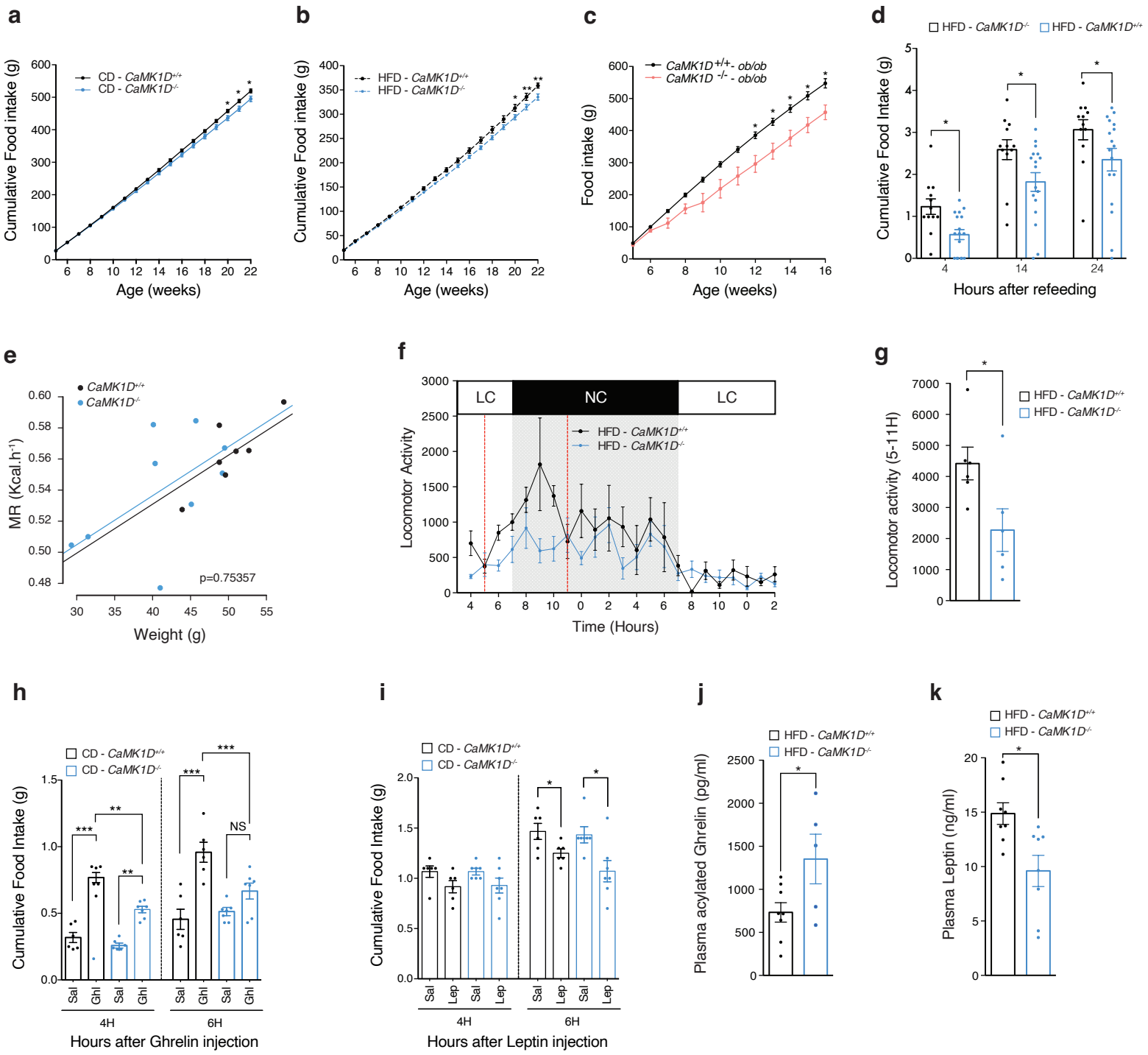
a
Cumulative Food intake (g)
CD - CaMK1D+/+
CD - CaMK1D-/-
Age (weeks)
b
Cumulative Food intake (g)
HFD - CaMK1D+/+
HFD - CaMK1D-/-
Age (weeks)
c
Food intake (g)
CaMK1D +/+ - ob/ob
CaMK1D -/- - ob/ob
Age (weeks)
d
HFD - CaMK1D-/-
HFD - CaMK1D+/+
Cumulative Food Intake (g)
Hours after refeeding
e
CaMK1D+/+
CaMK1D-/-
MR (Kcal.h-1)
p=0.75357
Weight (g)
f
LC
NC
LC
HFD - CaMK1D+/+
HFD - CaMK1D-/-
Locomotor Activity
Time (Hours)
g
HFD - CaMK1D+/+
HFD - CaMK1D-/-
Locomotor activity (5-11H)
h
CD - CaMK1D+/+
CD - CaMK1D-/-
Cumulative Food Intake (g)
Sal
Ghl
4H
6H
Hours after Ghrelin injection
i
CD - CaMK1D+/+
CD - CaMK1D-/-
Cumulative Food Intake (g)
Sal
Lep
4H
6H
Hours after Leptin injection
j
HFD - CaMK1D+/+
HFD - CaMK1D-/-
Plasma acylated Ghrelin (pg/ml)
k
HFD - CaMK1D+/+
HFD - CaMK1D-/-
Plasma Leptin (ng/ml)

Figure 3

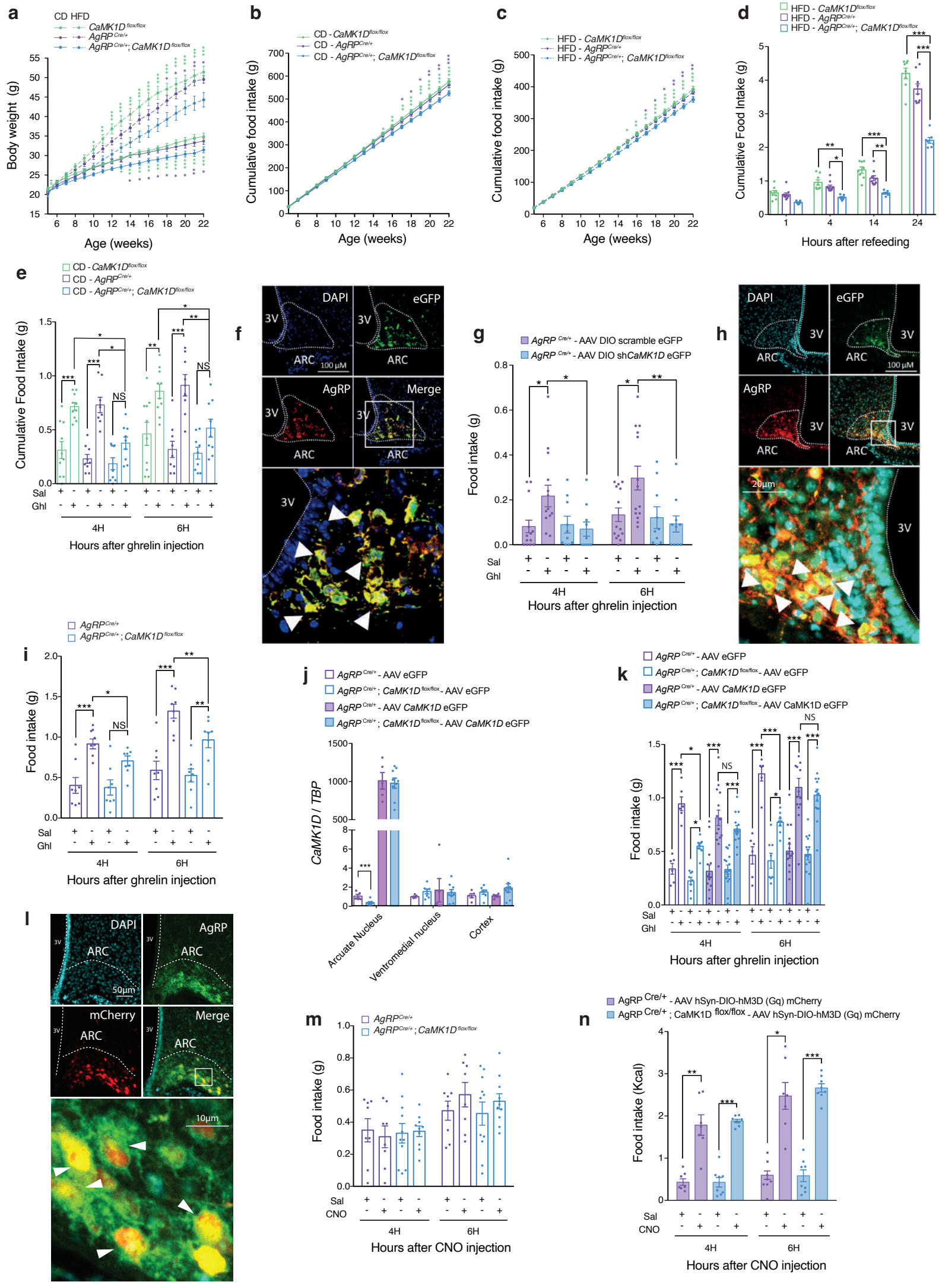
a
CD HFD
CaMK1D flox/flox
AgRP Cre/+
AgRP Cre/+; CaMK1D flox/flox
Body weight (g)
Age (weeks)
b
CD - CaMK1D flox/flox
CD - AgRP Cre/+
CD - AgRP Cre/+; CaMK1D flox/flox
Cumulative food intake (g)
Age (weeks)
c
HFD - CaMK1D flox/flox
HFD - AgRP Cre/+
HFD - AgRP Cre/+; CaMK1D flox/flox
Cumulative food intake (g)
Age (weeks)
d
HFD - CaMK1D flox/flox
HFD - AgRP Cre/+
HFD - AgRP Cre/+; CaMK1D flox/flox
Cumulative Food Intake (g)
Hours after refeeding
e
CD - CaMK1D flox/flox
CD - AgRP Cre/+
CD - AgRP Cre/+; CaMK1D flox/flox
Cumulative Food Intake (g)
Sal
Ghl
4H
6H
Hours after ghrelin injection
f
DAPI
eGFP
AgRP
Merge
3V
ARC
100 µM
g
AgRP Cre/+ - AAV DIO scramble eGFP
AgRP Cre/+ - AAV DIO shCaMK1D eGFP
Food intake (g)
Sal
Ghl
4H
6H
Hours after ghrelin injection
h
DAPI
eGFP
AgRP
3V
ARC
100 µM
20µm
i
AgRP Cre/+
AgRP Cre/+ ; CaMK1D flox/flox
Food intake (g)
Sal
Ghl
4H
6H
Hours after ghrelin injection
j
AgRP Cre/+ - AAV eGFP
AgRP Cre/+ ; CaMK1D flox/flox - AAV eGFP
AgRP Cre/+ - AAV CaMK1D eGFP
AgRP Cre/+ ; CaMK1D flox/flox - AAV CaMK1D eGFP
CaMK1D / TBP
Arcuate Nucleus
Ventromedial nucleus
Cortex
k
AgRP Cre/+ - AAV eGFP
AgRP Cre/+ ; CaMK1D flox/flox - AAV eGFP
AgRP Cre/+ - AAV CaMK1D eGFP
AgRP Cre/+ ; CaMK1D flox/flox - AAV CaMK1D eGFP
Food intake (g)
Sal
Ghl
4H
6H
Hours after ghrelin injection
l
DAPI
AgRP
mCherry
Merge
3V
ARC
50µm
10µm
m
AgRP Cre/+
AgRP Cre/+ ; CaMK1D flox/flox
Food intake (g)
Sal
CNO
4H
6H
Hours after CNO injection
n
AgRP Cre/+ - AAV hSyn-DIO-hM3D (Gq) mCherry
AgRP Cre/+ ; CaMK1D flox/flox - AAV hSyn-DIO-hM3D (Gq) mCherry
Food intake (Kcal)
Sal
CNO
4H
6H
Hours after CNO injection

Figure 4

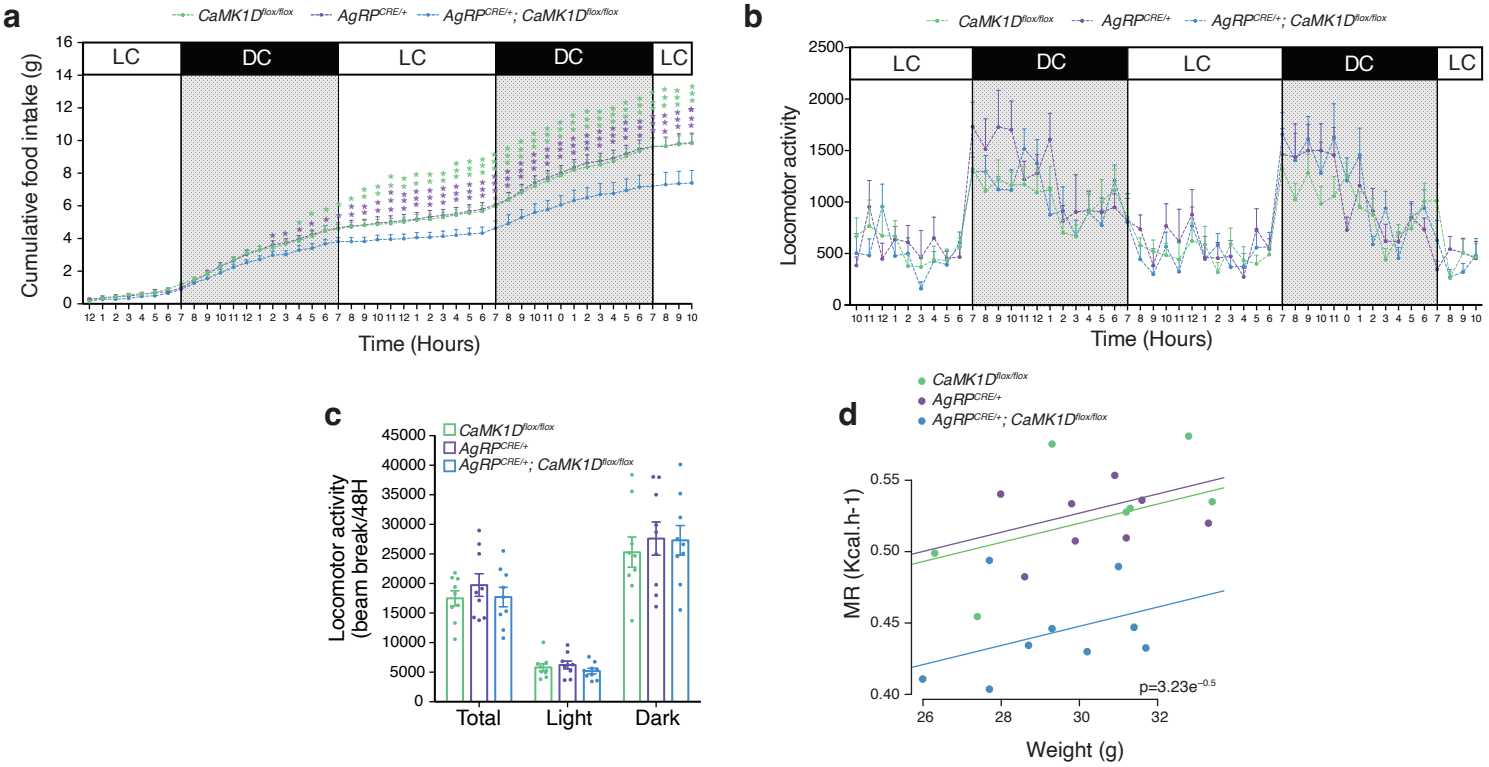
a
CaMK1D flox/flox
AgRP CRE/+
AgRP CRE/+; CaMK1D flox/flox
LC
DC
LC
DC
LC
Cumulative food intake (g)
Time (Hours)
b
CaMK1D flox/flox
AgRP CRE/+
AgRP CRE/+; CaMK1D flox/flox
LC
DC
LC
DC
LC
Locomotor activity
Time (Hours)
c
CaMK1D flox/flox
AgRP CRE/+
AgRP CRE/+; CaMK1D flox/flox
Locomotor activity (beam break/48H
Total
Light
Dark
d
CaMK1D flox/flox
AgRP CRE/+
AgRP CRE/+; CaMK1D flox/flox
MR (Kcal.h-1)
p=3.23e−0.5
Weight (g)

Figure 5

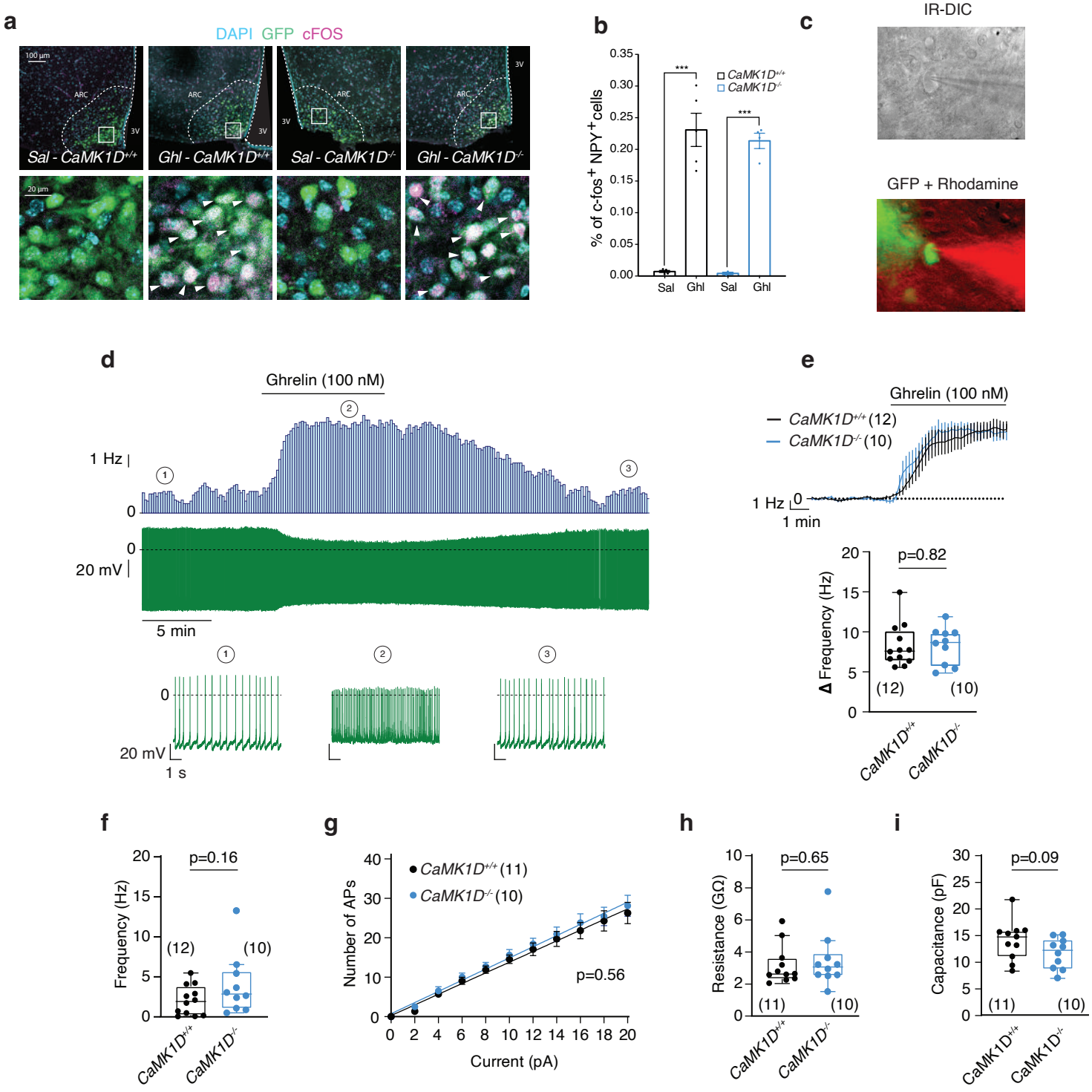
a
DAPI GFP cFOS
100 µm
ARC
3V
Sal - CaMK1D+/+
Ghl - CaMK1D+/+
Sal - CaMK1D-/-
Ghl - CaMK1D-/-
20 µm
b
% of c-fos+ NPY+ cells
0.35
0.30
0.25
0.20
0.15
0.10
0.05
0.00
***
***
CaMK1D+/+
CaMK1D-/-
Sal
Ghl
Sal
Ghl
c
IR-DIC
GFP + Rhodamine
d
Ghrelin (100 nM)
1 Hz
0
20 mV
5 min
1
2
3
1 s
e
Ghrelin (100 nM)
CaMK1D+/+ (12)
CaMK1D-/- (10)
1 Hz
1 min
Δ Frequency (Hz)
p=0.82
(12)
(10)
f
Frequency (Hz)
p=0.16
(12)
(10)
g
Number of APs
CaMK1D+/+ (11)
CaMK1D-/- (10)
p=0.56
Current (pA)
h
Resistance (GΩ)
p=0.65
(11)
(10)
i
Capacitance (pF)
p=0.09
(11)
(10)